



Tropospheric bromine monoxide in Ny-Ålesund: source analysis and impacts on atmospheric chemistry

Qidi Li^{1,2,3}, Yuhan Luo^{1*}, Xin Yang^{3*}, Bianca Zilker⁴, Andreas Richter⁴, Ke Dou¹, Haijin Zhou¹, Kai Zhan¹, Fuqi Si¹ and Wenqing Liu¹

¹Key Laboratory of Environmental Optics and Technology, Anhui Institute of Optics and Fine Mechanics, Hefei Institutes of Physical Science, Chinese Academy of Sciences, Hefei, China

²University of Science and Technology of China, Hefei, China

³British Antarctic Survey, Natural Environment Research Council, Cambridge, UK

⁴Institute of Environmental Physics, University of Bremen, Bremen, Germany

Correspondence to: Yuhan Luo (yhluo@aiofm.ac.cn) and Xin Yang (xinyang55@bas.ac.uk)

Abstract. Arctic tropospheric bromine monoxide (BrO) plays a critical role in atmospheric chemistry, particularly during springtime ozone depletion events. While sources such as sea ice, open ocean, aerosols, and snowpack have been proposed, their relative contributions remain uncertain. In this study, we addressed this uncertainty using long-term Multi-Axis Differential Optical Absorption Spectroscopy observations of BrO and aerosol profiles in Ny-Ålesund, Svalbard (78.92°N, 11.93°E), collected during March-May 2017–2023. Supporting datasets included Global Ozone Monitoring Experiment-2B BrO satellite retrievals, Hybrid Single-Particle Lagrangian Integrated Trajectory back trajectories, and sea salt aerosol (SSA) simulations from a Chemistry transport model (p-TOMCAT). We found a strong correlation between BrO volume mixing ratios and aerosol extinction, suggesting a close association between BrO enhancements and airborne particles. Five-day backward trajectories (0-3 km) showed significant BrO correlation with sea ice contact time, particularly under strong winds. Observed BrO also correlated with modelled blowing-snow-sourced SSA concentrations and bromine emission fluxes from blowing snow. During bromine explosion events (BEEs), air mass contact with sea ice (52.0% of all trajectories, 0-3 km) far exceeded that with open ocean (6.8%), highlighting sea ice as the dominant bromine source. Within the boundary layer (< 500 m), multi-year ice contributed more than first-year ice (56.1% vs. 23.8%) during BEEs, underscoring its importance. Snowpack-sourced bromine fluxes also correlated with BrO, although disentangling release processes remains challenging. These results provide long-term observational evidence linking BrO to sea-ice and SSA processes, advancing understanding of Arctic bromine activation and its implications for springtime ozone depletion.

30 1 Introduction

Reactive bromine plays a crucial role in the Arctic troposphere (Barrie et al., 1988). In polar spring, the release of large amounts of reactive bromine species (Br and BrO) during bromine explosion events (BEEs) (Wennberg, 1999; Abbatt et al., 2012; Simpson et al., 2007a) can trigger ozone depletion events (ODEs), in which surface ozone volume mixing ratios (VMRs) fall



45

50



below 10 ppbv and sometimes approach near-zero values (Oltmans and Komhyr, 1986; Bottenheim et al., 1986; Halfacre et al., 2014). Reactive bromine also influences key photochemical species in the boundary layer, including OH/HO₂, NO/NO₂, and volatile organic compounds (Barrie and Platt, 1997; von Glasow and Crutzen, 2007; Simpson et al., 2015). Furthermore, enhanced reactive bromine promotes the oxidation of gaseous elemental mercury (GEM) and increases the deposition of particulate mercury, potentially impacting Arctic wildlife and human health through bioaccumulation in the food chain (Schroeder et al., 1998; Steffen et al., 2008).

In ozone depletion chemistry, the three main reaction cycles involving reactive bromine—self-reaction (BrO + BrO), cross-reaction (BrO + IO/ClO), and the catalytic cycle (BrO + HO₂)—do not modify the total abundance of the Br_x family (Simpson et al., 2007a). BEEs are widely believed to occur through heterogeneous reactions on low-pH saline surfaces containing sufficient bromide (Br⁻), which release reactive bromine into the gas phase via an autocatalytic cycle (Fan and Jacob, 1992; Wennberg, 1999; Abbatt et al., 2012):

$$HOBr + Br^{-}(aq) + H^{+}(aq) \rightarrow Br_2 + H_2O$$
(R1)

$$Br_2 + h\nu \to 2Br \tag{R2}$$

$$Br + O_3 \rightarrow BrO + O_2 \tag{R3}$$

$$BrO + HO_2 \rightarrow HOBr + O_2$$
 (R4)

In the multiphase reaction R1, HOBr reacts with Br⁻, releasing a bromine molecule. Photolysis of Br₂ (R2) produces two bromine atoms, leading to a rapid buildup of reactive bromine (Lehrer et al., 2004). In addition to this pathway, other bromine release mechanisms have been reported. For example, at night, the reaction between O₃ and bromide ions on saline surfaces can generate gaseous bromine molecules (Oum et al., 1998). Laboratory studies have shown that bromide ions, H₃O⁺, and O₂ can produce bromine radicals through heterogeneous reactions under nighttime conditions (Cao et al., 2024). Furthermore, the release of reactive bromine could also be influenced by sea salt Cl⁻ (Vogt et al., 1996) and OH radicals (Halfacre et al., 2019). Potential sources of reactive bromine include: open ocean sea spray (Sander et al., 2003), first-year sea ice (Jones et al., 2006; Simpson et al., 2007b), multi-year sea ice (Peterson et al., 2019; Huang et al., 2020), frost flowers (Kaleschke et al., 2004; Nghiem et al., 2012), sea salt aerosol (SSA) from polynyas or open leads (Kirpes et al., 2019; Criscitiello et al., 2021), snowpack photochemistry (Toyota et al., 2011, 2014; Pratt et al., 2013), blowing-snow-sourced SSA (Yang et al., 2008, 2010; Jones et al., 2009; Choi et al., 2018; Huang et al., 2020), and stratosphere-to-troposphere transport of BrO (Salawitch et al., 2010).

Investigating reactive bromine release mechanisms in the polar troposphere requires robust observational evidence, which has been partially provided by satellite measurements offering key insights into BrO distribution. Wagner and Platt (1998) and Richter et al. (1998) reported elevated BrO in the polar spring from GOME measurements, with BrO-rich air masses generally located near sea ice regions. Jacobi et al. (2006) reported enhanced tropospheric BrO detected by the SCIAMACHY satellite during an ODE near the Arctic sea ice edge. Jones et al. (2009) observed elevated BrO with SCIAMACHY at Halley Station, Antarctica, and found that both stable boundary layers under low wind speeds and turbulent boundary layers under high wind



70

100



speeds could lead to ODEs. Subsequent studies using GOME-2 satellite observations linked Arctic BrO enhancement to high-wind cyclonic systems, blowing-snow-generated SSA, and first-year sea ice contact (Begoin et al., 2010; Theys et al., 2011; Bougoudis et al., 2020). Seo et al. (2019) detected BrO enhancements with TROPOMI in diverse regions, including Arctic sea ice, volcanic areas, and salt lakes. However, limited spatial resolution and vertical sensitivity hinder a full understanding of reactive bromine activation mechanisms (Sihler et al., 2012).

Ground-based Differential Optical Absorption Spectroscopy (DOAS) observations provide minute-level temporal resolution and good vertical coverage, offering significant advantages for studying boundary layer BEEs (Hausmann and Platt, 1994; Hönninger et al., 2004; Frieß et al., 2004, 2011; Liao et al., 2011; Stutz et al., 2011; Peterson et al., 2015; Zhao et al., 2016; Simpson et al., 2017). Enhanced BrO has been detected during polar spring using long-path DOAS and MAX-DOAS instruments (Hausmann and Platt, 1994; Hönninger et al., 2004). MAX-DOAS observations also facilitate investigations of BrO vertical distribution within the boundary layer (Peterson et al., 2015; Simpson et al., 2017; Frieß et al., 2023; Brockway et al., 2024). Additionally, BrO has been measured using airborne DOAS instruments and chemical ionization mass spectrometers, although such measurements are generally limited to specific campaigns (Liao et al., 2011, 2012; General et al., 2014; Peterson et al., 2017).

Based on these observations, various reactive bromine emission mechanisms have been incorporated into chemical models. For example, Toyota et al. (2011, 2014) implemented a chemical scheme representing reactive bromine release from snowpack on sea ice, successfully reproducing enhanced BrO observed by the GOME satellite during Arctic spring. The same mechanism has also been applied to simulate BrO in both the Arctic and Antarctic (Falk and Sinnhuber, 2018). Yang et al. (2008, 2010) developed an alternative scheme in which reactive bromine is released from SSA generated by blowing snow, rather than directly from snowpack emissions. This mechanism is supported by recent field observations confirming SSA production from blowing snow (Yang et al., 2019; Frey et al., 2020; Gong et al., 2023). Models using this scheme have successfully reproduced BEEs and ODEs in both hemispheres. For instance, Choi et al. (2018) reported that the spatial distribution of model-simulated SSA from blowing snow closely matched tropospheric BrO columns observed by the OMI satellite during Arctic spring. Similarly, Huang et al. (2020) simulated numerous BEEs in the Arctic during March and April of 2007–2009 and found that blowing snow over multi-year sea ice could be an important reactive bromine source. Marelle et al. (2021) modelled Arctic ODEs in spring 2012 by applying both the snowpack and blowing-snow SSA schemes, and their results indicated that each contributed to ODE occurrence. Although these models can reproduce BEEs and ODEs, challenges remain due to low spatial resolution, limited ability to simulate boundary layer dynamics, and a lack of field data to constrain key parameters such as snow salinity and snow age, making quantitative comparison with in situ observations and mechanism validation difficult. Driven by global warming and Arctic amplification, Arctic sea ice has been significantly altered over the past three decades,

with both its extent and thickness decreasing (Comiso et al., 2017; Bocquet et al., 2024). During polar spring, the region north of Ny-Ålesund is typically covered by sea ice, whereas the area to the south is generally open ocean. This sharp geographical contrast provides a natural laboratory for investigating the relative contributions of open ocean and sea ice to reactive bromine emissions. In Ny-Ålesund, several research groups have conducted BrO observations over the years. Tuckermann et al. (1997)



105

110

115

120



detected BrO VMR exceeding 30 pptv using a DOAS instrument, which were associated with severe ODEs. Langendörfer et al. (1999) reported that filterable bromine concentrations measured by ion chromatography were consistent with BrO variations observed by DOAS. Luo et al. (2018) reported that enhanced BrO detected by MAX-DOAS in April 2015 was linked to sea ice cover in the Kings Bay region. Chen et al. (2022) documented a BEE event in March 2017, observed by MAX-DOAS, and attributed it primarily to SSA generated by blowing snow over sea ice under high wind conditions. Zilker et al. (2023) analyzed surface ozone and satellite-retrieved tropospheric BrO column data during spring seasons from 2010 to 2021, showing that enhanced BrO frequently occurred near Svalbard during ODEs, with the strongest enhancements typically observed in March. The primary sources of reactive bromine during BEEs remain uncertain. Field studies in Alaska and laboratory experiments have shown that acidic saline snowpacks can release reactive bromine when exposed to sunlight and ozone (Wren et al., 2013; Pratt et al., 2013). Reactive bromine fluxes from snowpack in Alaska, ranging from 7 × 10⁷ to 1.2 × 10⁹ molecules cm⁻² s⁻¹, based on direct measurements of BrCl and Br2, were reported, with values consistent with those used in models to reproduce BEEs and ODEs (Custard et al., 2017). In contrast, Yang et al. (2024) derived a much lower average (monthly timescale) snowpack release flux of 1×10^7 molecules cm⁻² s⁻¹ or below from field measurements in Eureka, Canada (86.4°W, 80.1°N), suggesting that coastal snowpack is a weak reactive bromine source. Moreover, based on a mass balance approach, Yang et al. (2024) estimated that the lifetime of atmospheric reactive bromine as a family is 17–42 days, which is longer than the 4–10 days reported in previous studies (von Glasow et al., 2004; Yang et al., 2005). Ground-based DOAS observations at Neumayer Station, Antarctica, and Barrow Station, Arctic, have indicated that first-year sea ice plays a potentially significant role as a source (Frieß et al., 2004; Simpson et al., 2007b). Enhanced BrO over first-year sea ice has also been observed by LP-DOAS in the Amundsen region (Pöhler et al., 2010). Furthermore, DOAS measurements have associated enhanced BrO with increased aerosol extinction under high wind speeds (Bognar et al., 2020). Fresh frost flowers, although highly alkaline and saline, likely make only minor or local contributions due to their limited spatial extent on open leads (Obbard et al., 2009; Lieb-Lappen and Obbard, 2015). Stratospheric influence on tropospheric BrO columns also appears limited (Theys et al., 2011).

In this study, we retrieved 0–4 km BrO partial columns from observations made using a MAX-DOAS deployed at the Yellow River Station in Ny-Ålesund during 2017–2023. These data were combined with overpassing GOME-2B satellite measurements, p-TOMCAT model simulations, near-surface ozone observations, local meteorological records, and backward trajectories to study the possible sources and causes of variability in BrO levels in Ny-Ålesund. We further quantified the relative contributions of open ocean and sea ice to reactive bromine. Section 2 describes the methods and data used in this analysis. The results and discussions are presented in Section 3, and the conclusions are summarized in Section 4.

2 Data and Methods

2.1 Location

In this study, BrO partial columns and aerosol extinction were measured at the Arctic Yellow River Station in Ny-Ålesund (78.92° N, 11.93° E; 10 m above sea level [asl]), located on the western coast of Svalbard, with the instrument installed at an





altitude of 30 m asl. As shown in Figure 1, the area southwest of Svalbard is predominantly open ocean due to the North Atlantic Warm Current. First-year sea ice mainly covers the Barents Sea to the east, whereas multi-year sea ice dominates areas northwest of Svalbard and near Greenland. Meteorological data from the Ny-Ålesund atmospheric observatory were supplied by the Alfred Wegener Institute–Research Unit Potsdam and accessed through the PANGAEA database (Maturilli, 2018–2023). This study used meteorological records for March–May during the years 2017–2023. Continuous ozone and GEM measurements have been carried out at Zeppelin Station (78.54° N, 11.53° E; 474 m asl). These datasets were obtained from the EBAS database managed by the Norwegian Institute for Air Research (https://ebas-data.nilu.no/).

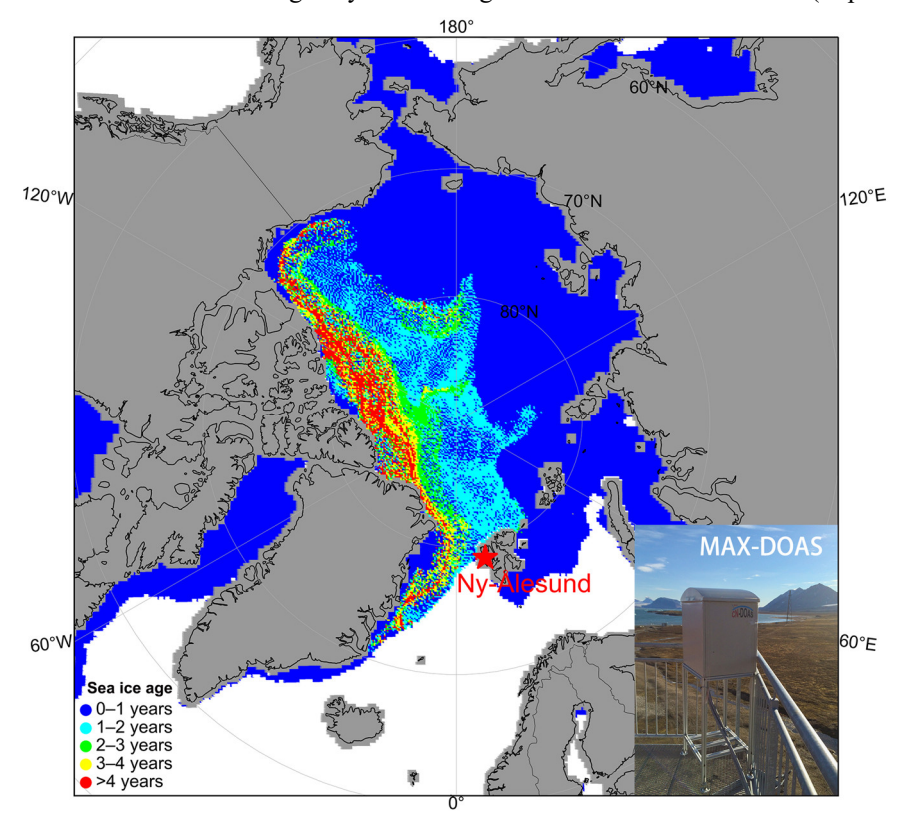


Figure 1. Location of the MAX-DOAS observations at Ny-Ålesund. The background map shows the distribution of sea ice age during March 11–17, 2020, based on weekly sea ice age data (https://daacdata.apps.nsidc.org/). Different colours represent sea ice of various ages, from first-year sea ice to multi-year sea ice, while white areas indicate open ocean.

2.2 Remote sensing data

2.2.1 MAX-DOAS

145

150

A MAX-DOAS instrument has been installed at the Chinese Yellow River Station in Ny-Ålesund since April 2015, with an azimuthal viewing direction of 45°. It collects scattered sunlight from multiple viewing angles using an outdoor telescope, which is connected via optical fiber to an indoor spectrometer (Ocean Optics MAYA Pro). The spectrometer transmits spectral



160

165

170



data to a computer for processing through a CCD detector. A temperature controller maintains the spectrometer at 20 °C to ensure the stability of its optical properties. The instrument covers a wavelength range of 290–429 nm, with a full width at half maximum (FWHM) resolution of 0.5 nm. The MAX-DOAS operates at elevation angles of 2°, 3°, 4°, 6°, 8°, 10°, 15°, 30°, and 90°, requiring approximately 15 minutes to complete a full measurement sequence. The integration time for each spectrum varies depending on incident light intensity.

The spectral data were processed with QDOAS software, which applied the DOAS technique (Platt and Stutz, 2008; Danckaert et al., 2017). Differential Slant Column Densities (DSCDs) of BrO and O₄ were retrieved using the parameter settings listed in Table 1. Reference spectra for the retrievals were taken from observations towards the zenith within each measurement sequence. Only spectra with a solar zenith angle (SZA) less than 86° were included in the analysis.

Table 1. MAX-DOAS spectral setting for BrO and O₄ analysis.

Parameters	BrO	O ₄
O ₃ _223K (Bogumil et al., 2003)	√	√
O ₃ _243K (Bogumil et al., 2003)	\checkmark	
NO _{2_298K} (Vandaele et al., 1998)	\checkmark	\checkmark
NO ₂ _220K (Vandaele et al., 1998)	\checkmark	\checkmark
O ₄ _273K (Thalman and Volkamer, 2013)	\checkmark	\checkmark
BrO_298K (Fleischmann et al., 2004)	\checkmark	N/A
OCIO_233K (Kromminga et al., 2003)	\checkmark	N/A
Ring (Calculated with QDOAS)	\checkmark	\checkmark
Wavelength	336.5–359 nm	340–370 nm
Polynomial	Fifth order	Fifth order

The BrO and aerosol extinction vertical profiles were retrieved using the HEIPRO algorithm, which is based on the Optimal Estimation Method (OEM) (Rodgers, 2000; Frieß et al., 2006, 2011). In this retrieval, the most probable atmospheric state was determined by minimizing the cost function χ^2 , expressed as:

$$\chi^{2} = (y - F(x, b))^{T} S_{\epsilon}^{-1} (y - F(x, b)) + (x - x_{a})^{T} S_{a}^{-1} (x - x_{a})$$
 (R5)

Here, the measurement vector y represents the observed DSCDs of BrO and O₄. The function F(x, b) denotes the atmospheric radiative transfer model (SCIATRAN, Rozanov et al., 2005), where x refers to the retrieved BrO and aerosol extinction vertical profiles, and b refers to meteorological parameters including pressure and temperature. The pressure and temperature profile data were obtained from climatological databases (Brühl and Crutzen, 1993). x_a denotes the a priori state vector, while S_ϵ and S_a are covariance matrices representing the uncertainties of the measurement and a priori states, respectively. In the retrieval, key parameters for evaluating the results are the averaging kernel matrix ($A = \partial \hat{x}/\partial x$) and the degrees of freedom for signal



180

185

190



(DOFS). The averaging kernel matrix A describes the sensitivity of the retrieved profile to the true atmospheric state, while the DOFS, defined as the sum of the diagonal elements of A, quantifies the amount of independent information in the retrieval. Following the approach of Frieß et al. (2011), a two-step retrieval was applied. The aerosol extinction profile was first derived from the observed O₄ DSCDs and subsequently used as input for the forward model to retrieve the vertical profile of BrO. In both steps, SCIATRAN was used as the forward model.

A vertical 200 m-resolution grid was employed to retrieve aerosol extinction and BrO profiles, covering altitudes up to 4 km with a total of 20 vertical layers. The surface albedo was set to 0.1 (Chen et al., 2022). The a priori aerosol extinction profile followed an exponential distribution with a surface extinction of 0.05 km⁻¹ and a scale height of 2 km. Similarly, the a priori BrO profile was exponential, with a surface concentration of 1×10^9 molecules cm⁻³ and a scale height of 0.7 km. For both profiles, the a priori uncertainty was set to 100% of the a priori value, and the vertical correlation length was 0.5 km. To ensure sufficient information content in the retrievals, only results with DOFS greater than 0.7 for both aerosol and BrO were retained (Peterson et al., 2015; Bognar et al., 2020). The 0–4 km BrO partial columns, obtained by integrating the vertical profile within this altitude range, reliably represented the amount and variability of BrO observed from the MAX-DOAS instrument (Zhao et al., 2016; Bognar et al., 2020). Figure 2 shows the averaging kernels for aerosol and BrO under clear-sky conditions. Below 2 km, the retrievals of both aerosol and BrO exhibits good sensitivity, with peak averaging kernel values of approximately 0.8 near the surface. Above 2 km, the averaging kernel for BrO is very small, indicating low sensitivity to the true atmospheric state and a stronger influence of the a priori profile in this altitude range. The DOFS values were 2.80 for the aerosol extinction profile and 2.25 for the BrO profile, indicating that a substantial amount of independent information was obtained from the MAX-DOAS observations.

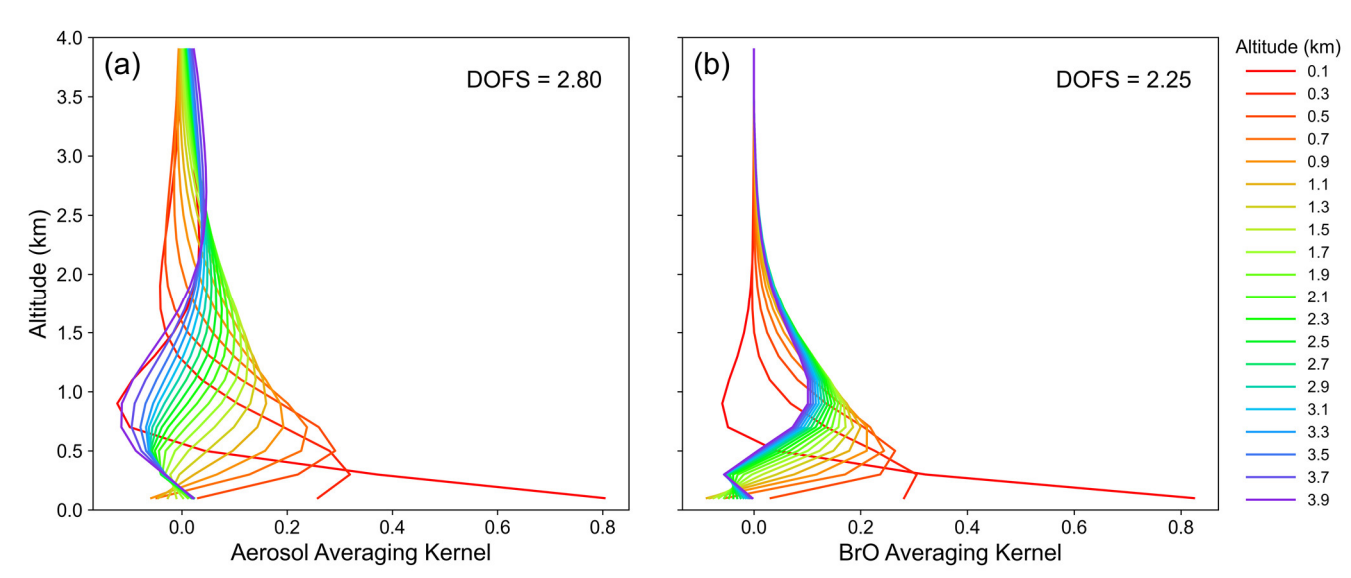






Figure 2. Averaging kernels for aerosol (a) and BrO (b) at 10:22 UTC on April 2, 2020. The aerosol optical depth (AOD) is 7.73×10^{-2} . The DOFS are 2.80 for the aerosol extinction profile and 2.25 for the BrO profile. Curves of different colours represent the averaging kernels at different altitude layers.

2.2.2 GOME-2B

195

200

205

210

215

The BrO tropospheric Vertical Column Densities (VCD_{trop}) from the Global Ozone Monitoring Experiment–2B (GOME-2B) were retrieved according to Bougoudis et al. (2020). The total Slant Column Densities (SCDs) of BrO were retrieved using the DOAS method (Burrows et al., 2011) with a fitting window of 338-360 nm. Stratospheric correction was applied according to Theys et al. (2009). This O₃, NO₂, and time depending climatology of stratospheric BrO vertical columns was derived with the BASCOE model (Errera and Fonteyn, 2001). Using a stratospheric air mass factor, the stratospheric BrO slant column was derived and subtracted from the total slant column to obtain the tropospheric BrO slant column. Finally, a tropospheric air mass factor was applied to derive the BrO VCD_{trop}. The GOME-2B satellite crosses the equator at 09:30 local time, with a spatial resolution of 80 km × 40 km (Bougoudis et al., 2020). In polar regions, extreme observational geometry enhances scattering and attenuation, resulting in reduced radiance signals. According to Bougoudis et al. (2020), the daily average root mean square error (RMSE) of retrievals typically remained below 2.0×10^{-3} . The GOME-2B BrO VCD_{trop} values used in this study were those within 45 km of Ny-Ålesund. The GOME-2B BrO VCD_{trop} refers to the vertical column below the tropopause, which is typically located between 7.5 and 9.5 km in the Arctic, depending on meteorological conditions (Seo et al., 2020). The comparison between the 0-4 km BrO partial columns retrieved by MAX-DOAS and the GOME-2B BrO VCD_{trop} is presented in Fig. S1. As shown, there was a significant correlation between the MAX-DOAS and GOME-2B BrO observations, with a r of 0.74 (p < 0.001, N=506). On average, the GOME-2B BrO VCD_{trop} values are higher than the MAX-DOAS BrO partial columns by 1.28 × 10¹³ molecules cm⁻². This difference is at least partially explained by the fact that GOME-2B BrO represents the entire troposphere, whereas MAX-DOAS only captures the lowest 0-4 km. However, during periods of substantial BrO enhancement—such as 17-20 March 2017, 2-3 April 2019, and 16 and 23 March 2020—the MAX-DOAS BrO partial columns occasionally exceeded the GOME-2B BrO VCD_{trop}. This is likely due to the higher sensitivity of MAX-DOAS to near-surface BrO, while satellite observations may underestimate the enhancement of reactive bromine close to the surface (Sihler et al., 2012) or due to the low spatial resolution of GOME-2B.

2.3 Emission parameterisations

2.3.1 Blowing-snow-sourced emissions in p-TOMCAT model

The Cambridge Parallelised Tropospheric Offline Model of Chemistry and Transport (p-TOMCAT) is a global three-dimensional chemical transport model employed to study tropospheric chemistry. The model has a horizontal resolution of $2.825^{\circ} \times 2.825^{\circ}$ and a vertical structure comprising 31 layers. The mean altitude of the lowest layer is about 30 m, while the pressure at the top layer is about 10 hPa (~31 km). Meteorological fields driving the model—such as temperature, humidity ,wind speed, and humidity—were obtained from the 6-hourly ERA5 dataset provided by the European Centre for



225

230

235

240

245



Medium-Range Weather Forecasts (ECMWF). Monthly sea ice coverage and sea surface temperature were sourced from the Hadley Centre Sea Ice and Sea Surface Temperature dataset (Rayner et al., 2003). The tropospheric bromine chemistry scheme in the model was described in detail by Yang et al. (2005, 2010, 2020). The parameterization of SSA emissions from the open ocean followed the formulations of Gong et al. (2003) and Jaeglé et al. (2011), while SSA emissions from blowing snow over sea ice were based on the parameterizations of Yang et al. (2008, 2019). Snow salinity values used in the study were obtained from the MOSAiC measurements (Macfarlane et al., 2023). Model settings for representing blowing-snow-sourced bromine were identical to those used by Ranjithkumar et al. (2025), except for applying a mean snow age of 1.5 days. This snow age was shorter than the previously suggested 3 days for the Arctic (Huang et al., 2020), as measurements performed at Eureka, Canada, accounted for non-traceable precipitation events, which substantially increased precipitation frequency and consequently reduced surface snow age. The representation of SSAs from both open ocean and sea ice comprised 21 size bins, with particle diameters ranging from $0.02 \mu m$ to $12 \mu m$. In addition to model outputs of BrO and SSA, the same SSA production parameterization was applied along the back-trajectory track to calculate cumulative bromine emission fluxes for further analysis in Section 3.

2.3.2 Snowpack emissions

Following the approach of Toyota et al. (2011), the dry deposition flux of ozone over first-year sea ice snowpack was used to estimate the Br₂ emission flux. In this study, a simplified method was used to describe surface bromine emission flux, assuming a constant ozone concentration of 30 ppbv and a dry deposition velocity of 0.01 cm s^{-1} . As suggested, the Br₂ yield depended on the SZA: a value of 0.001 was used when the SZA exceeded 85° , and 0.075 was applied when the SZA was less than or equal to 85° . The calculated emission flux was then combined with back-trajectory results (Section 2.4) to estimate cumulative emission fluxes under different conditions for further analysis in Section 3. Four experimental groups were designed to investigate reactive bromine release under varying environmental conditions. The first group ($F_{br_snow_FYI}$) represents reactive bromine emissions over first-year sea ice when air temperature < -10 °C. The second group ($F_{br_snow_Seaice}$) is identical to the first but includes both multi-year and first-year sea ice. The third group ($F_{br_snow_\leqslant 7 \text{ m s}^{-1}}$) is identical to the second but restricted to low wind speeds ($\leqslant 7 \text{ m s}^{-1}$). Finally, the fourth group ($F_{br_snow_> 7 \text{ m s}^{-1}}$) is identical to the third but applied only to high wind speeds ($\gt 7 \text{ m s}^{-1}$).

2.4 Airmass trajectory model and analyses

250 The Hybrid Single-Particle Lagrangian Integrated Trajectory model (HYSPLIT) (Stein et al., 2015) was employed to investigate the sources of reactive bromine during BEEs in Ny-Ålesund. A BrO VMR greater than 12 pptv was used as the threshold for defining a BEE occurrence (Schofield et al., 2006). Meteorological data for driving the model were provided from the Global Data Assimilation System (GDAS) at a spatial resolution of 1° × 1° (Kleist et al., 2009). The HYSPLIT model





computed 120-hour backward trajectories of air masses arriving at Ny-Ålesund. Hourly backward trajectories were generated 255 with endpoints at 15 vertical levels below 3 km, with the lowest level at 100 m and subsequent levels at 200 m intervals. For each trajectory, the contact time of the air mass with various surface types—such as sea ice, open ocean, land, and free troposphere—was calculated. When the air mass was located below 500 m and encountered sea ice, open ocean, or land surfaces, the contact time with these surfaces was accumulated. If the air mass was above 500 m, it was considered to be in contact with the free troposphere. Sea ice age data were provided by the NASA National Snow and Ice Data Center (NSIDC) 260 (Tschudi et al., 2020), and sea ice concentration data from the ERA5 dataset (Hersbach et al., 2020). Sea ice older than one year was classified as multi-year ice, whereas ice younger than one year was classified as first-year ice. Sea ice concentration values ranged from 0 to 1, with values above 0.15 considered sea ice and values below 0.15 considered open ocean (Dukhovskoy et al., 2015). Along the trajectories, whenever the air mass encountered open ocean or sea ice surfaces (i.e., below 500 m), the corresponding bromine emission flux from SSA generated by open ocean and blowing snow was calculated 265 and accumulated by applying a given lifetime and weighting each hourly bromine emission flux F_{t_i} along the backward trajectory using an exponential decay factor $e^{-t_i/\tau}$, where t_i is the time in hours from the trajectory endpoint and τ is the lifetime of reactive bromine. In this study, τ was set to 5 days (120 hours, Yang et al., 2005). The total accumulated emission flux F was therefore calculated as:

$$F = \sum_{i=1}^{120} F_{t_i} \times e^{-t_i/\tau}$$
 (R6)

Here, 120 represents the total number of hourly points along the backward trajectory. A similar approach was applied to accumulate the reactive bromine emission flux from snowpack along the backward trajectories. In addition, a longer lifetime e.g., 30 days was also used to test the sensitivity of *F*, see discussion in section 3.4.

3 Results and discussions

3.1 Monthly variation of BrO, AOD, and Ozone

From the monthly results of BrO partial columns, AOD, and surface ozone in Fig. 3, it is evident that, despite clear year-to-year perturbations, March exhibits the highest BrO enhancement, while May records the lowest (Fig. 3a). This declining trend from March to May is reflected in all central-tendency metrics (mean, median, 75th, and 95th percentiles) (Fig. 3b). For example, the seven-year average decreasing rate is 2.7 × 10¹¹ molecules cm⁻² d⁻¹ from March to April and 1.23 × 10¹¹ molecules cm⁻² d⁻¹ from April to May, yielding an overall rate of 1.97 × 10¹¹ molecules cm⁻² d⁻¹ from March to May. This value is close to, but slightly smaller than, the Eureka 2019 rate of 3.03 × 10¹¹ molecules cm⁻² d⁻¹ (Yang et al., 2024). The mean inter-annual variability in the BrO partial column is largest in March, consistent with observations from Eureka, Canada (Bognar et al., 2020). In Ny-Ålesund, the BrO partial column in March 2020 is the highest, coinciding with high AOD and low surface ozone (Figs. 3c and 3e). By contrast, March 2018 exhibited an extremely low BrO partial column, accompanied



285

290

295

300



by low AOD and high surface ozone. Bognar et al. (2020) reported a similar phenomenon at Eureka, likely attributable to unusually calm weather conditions in March 2018.

The median AOD from March to May exhibits a slight downward trend (Fig. 3d). A detailed analysis of the relationship between BrO and aerosol extinction is provided in Section 3.4. At the monthly scale, surface ozone variations do not show a clear relationship with BrO partial columns. This was expected, as surface ozone is generally controlled by background ozone levels, except during BEEs that lead to ODEs, which occur only during a small fraction of the time. However, in certain months, BrO partial columns were closely associated with surface ozone. For instance, in March 2020, enhanced BrO partial columns corresponded to the lowest median and mean surface ozone values, whereas in March 2018, the lowest BrO partial columns coincided with higher surface ozone, close to background levels. Overall, median surface ozone decreases from March to May (Fig. 3f), consistent with the trend observed at Zeppelin Station during 1993–2019 (Law et al., 2023). This seasonality may be attributed to enhanced surface ozone photolysis, decreased NO_x emissions limiting photochemical ozone production, and potential effects of iodine compounds (Engvall Stjernberg et al., 2011; Schmale et al., 2018; Benavent et al., 2022), which are beyond the scope of this study.

The impact of bromine on surface ozone is also shown in Fig. 4. When surface ozone concentrations are low, the corresponding mean and median BrO partial columns are generally higher than those observed when ozone concentrations are high. Figure 4 presents boxplots of BrO partial columns categorized by different surface ozone concentration ranges (< 10, 10–15, 15–25, and > 25 ppbv). The highest mean and median BrO partial columns occur in the lowest ozone range (< 10 ppbv) and decrease progressively with increasing ozone concentrations. These results indicate that enhanced BrO partial columns are closely associated with the depletion of surface ozone, underscoring the key role of bromine chemistry in Arctic springtime atmospheric processes.





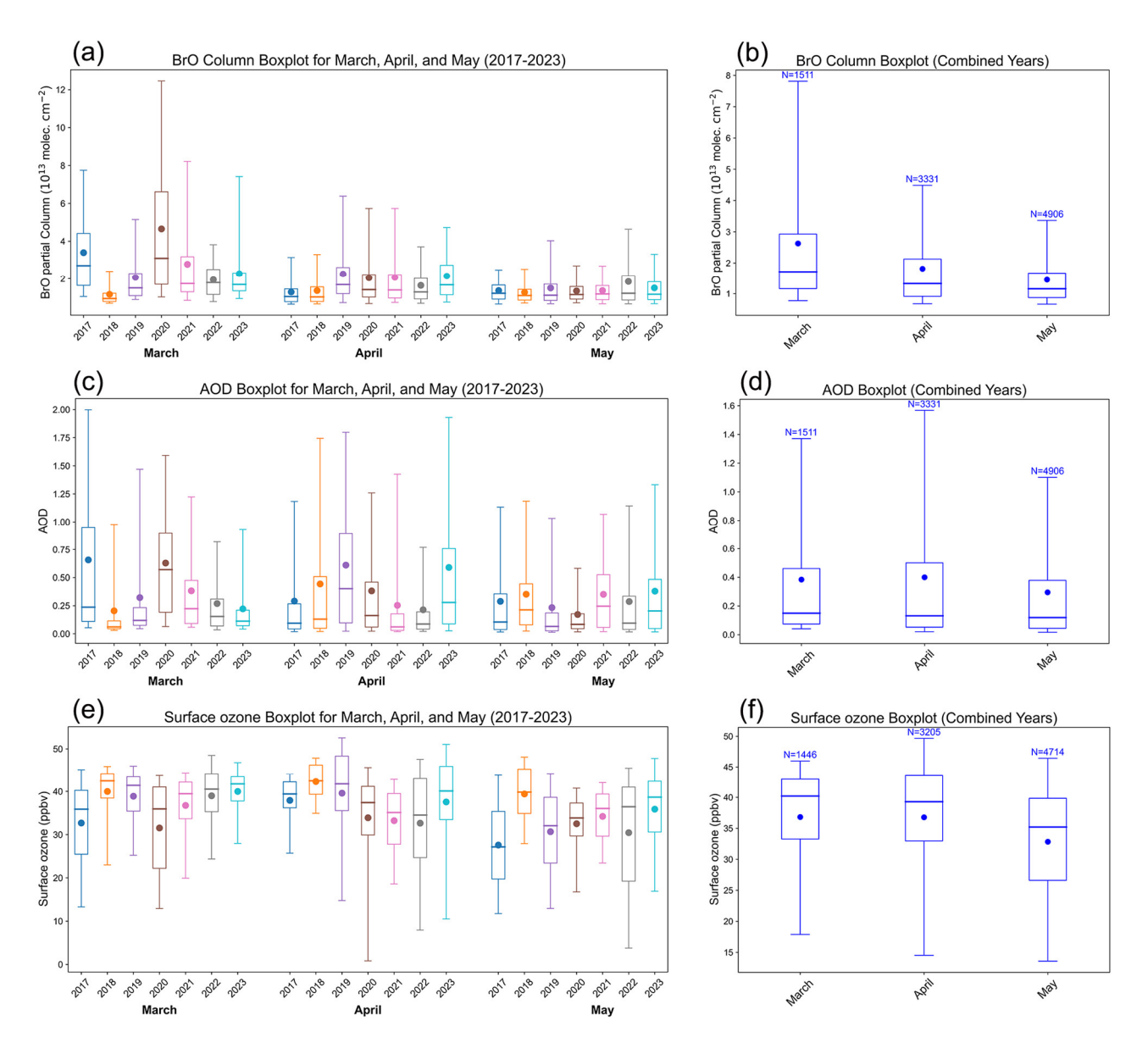


Figure 3. Left panel: boxplots of monthly BrO partial columns (a), AOD (c), and surface ozone (e) for March–May in each year from 2017 to 2023 in Ny-Ålesund; right panel: multiyear monthly BrO (b), AOD (d), and ozone (f). The boxes represent the 25th–75th percentile range, the whiskers indicate the 5th–95th percentile range, the dots represent the mean values, and the horizontal lines in the boxes indicate the median values. N is the number of hours counted. To ensure consistency with the MAX-DOAS BrO observations, only hours with valid surface ozone data during BrO observation periods were considered.



325



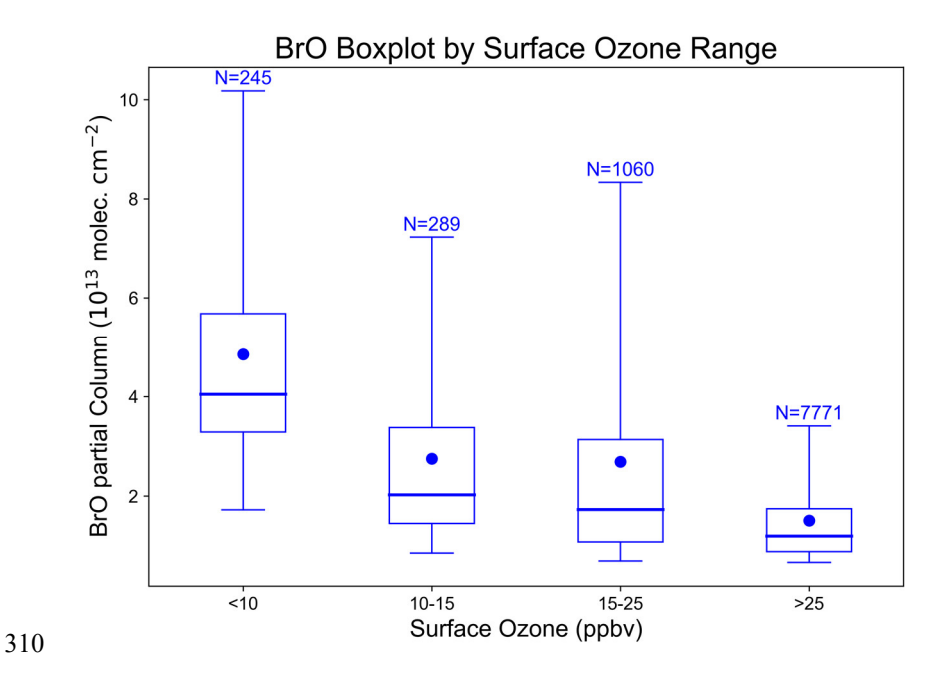


Figure 4. Boxplots of the BrO partial columns corresponding to surface ozone at different concentration ranges. Note that the data for surface ozone are from March to May for the 2017–2023 period. The boxes represent the 25th–75th percentile range, the whiskers indicate the 5th–95th percentile range, the dots represent the mean values, and the horizontal lines in the boxes indicate the median values. N is the number of hours counted.

315 3.2 Vertical distribution of BrO and aerosol extinction

The vertical distributions of BrO VMR at various SZA during March, April, and May are shown in Fig. 5, which presents the 95th percentile of the monthly BrO VMR. From March to May, BrO in Ny-Ålesund was primarily distributed below 2.5 km. In March, the 95th percentile of BrO VMR values exceeding 12 pptv was mainly observed below 900 m; in April, below 500 m; and in May, below 300 m, with maximum values generally occurring within the bottom 100 m. Over this period, the median, mean, and maximum BrO VMR values in the bottom 100 m layer gradually decreased; for example, the mean value declined from approximately 40 pptv in March to around 10 pptv in May (Figs. 5b, 5d, and 5f). Generally, BrO VMR decreased progressively with increasing altitude. Figure 5 shows a clear diurnal variation in BrO, with higher BrO VMR observed shortly after sunrise and before sunset, and a minimum around local noon. This pattern was generally in line with observations by Frieß et al. (2023) at the Neumayer and Arrival Heights stations. The noon minimum in BrO VMR is likely influenced by strong solar radiation, which enhances photochemical activity such as HO_2 production, thereby promoting BrO removal via the $HO_2 \to HOBr + O_2$ reaction (Pöhler et al., 2010). The morning enhancement of BrO is likely due to the nighttime accumulation of HOBr with HOBr which is photolyzed after sunrise to produce HOBr. The enhancement of HOBr before sunset is likely caused by the faster photolysis of HOBr compared with HOBr at dusk, followed by the reaction of bromine atoms with ozone; it is also promoted by the reduced efficiency of HOBr processes under low solar





radiation, both contributing to BrO accumulation (Buys et al., 2013). In addition, the stabilization of the boundary layer before sunset can further favour the accumulation of reactive bromine near the surface (Simpson et al., 2007).

High SZAs generally corresponded to data collected at the beginning of the month, whereas low SZAs corresponded to data collected at the end of the month. Given the clear decreasing trend in BrO VMR from March to May (Figure 3b), the reductions in BrO at lower SZA values (i.e., around local noon) may partly be attributable to the overall monthly decline in BrO. Another factor that could influence the diurnal variation is the number of profiles used in the analysis. For instance, in April, the number of profiles for each SZA bin gradually decreased from an SZA of 72° to 64°. A greatly reduced number of profiles could have introduced statistical uncertainty, for example, by lowering the 95th percentile BrO VMR. For this reason, Figure 5 presents only results derived from profiles where the number in each SZA bin exceeds 200.

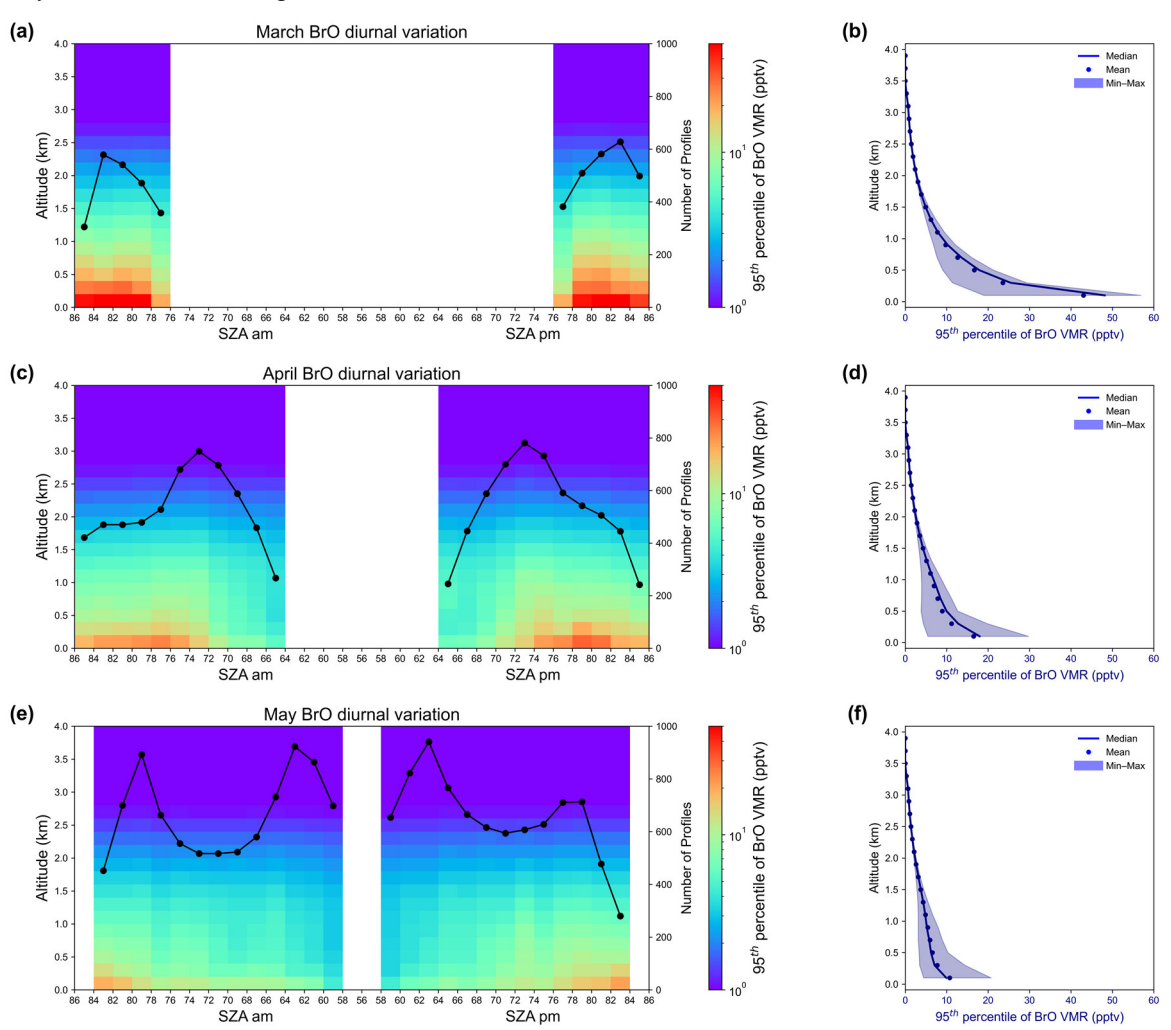


Figure 5. The 95th percentile vertical distributions of BrO VMR in Ny-Ålesund during spring (2017–2023) for March (a, b), April (c, d), and May (e, f), respectively. Panels (a, c, e) show vertical profiles of the 95th percentile BrO VMR as a function of SZA. The



350

355

360

365

370



black dots indicate the number of profiles (shown on the right y-axis) in each SZA bin; SZA bins with fewer than 200 profiles are excluded. Panels (b, d, f) show the statistical summary of the 95th percentile BrO VMR at each altitude across all SZA values: median (lines), mean (dots), and range (shaded area between minimum and maximum values), and BrO VMR is shown in blue.

345 **3.3 Typical Spring 2020**

3.3.1 The relation between BrO, aerosol, and air mass history

In this section, spring (March-May) 2020 was selected for detailed analysis because the number of BEE hours in March 2020 was the highest (~120 h) among all years (Fig. S2). This peak frequency made spring 2020 a particularly relevant period for investigating the relation between BrO, aerosols, and air mass history. BrO and aerosol extinction profiles, sea ice and openocean contact along air mass history trajectories, surface ozone, gaseous mercury, BrO partial column, and key meteorological parameters are presented in Fig. 6. The relationships between BrO and these parameters are presented in Fig. 7. BrO partial columns exhibits strong negative correlations with surface ozone (r = -0.51, p < 0.0001) and GEM (r = -0.44, p < 0.0001), supporting previous conclusions that enhanced BrO is associated with severe depletion of both ozone and GEM. Notably, BrO also exhibits negative correlations with key meteorological parameters, such as air temperature (r = -0.57, p < 0.0001) and pressure (r = -0.36, p < 0.0001). The temperature dependence may reflect the influence of temperature on bromine activation chemistry, as heterogeneous reactions leading to BrO release are more efficient at lower temperatures (Burd et al., 2017) or on air mass origin. Conversely, the strong negative correlation with air pressure suggests a role for atmospheric dynamical processes. For example, BrO shows a positive correlation with wind speed (r = 0.21, p < 0.0001), consistent with the proposed mechanism of reactive bromine release from blowing-snow-sourced SSA (Yang et al., 2008). These observed relationships are consistent with the discussion in Zilker et al. (2023), which focused on ozone depletion events in Ny-Ålesund and demonstrated a clear association with cold air masses originating from the central Arctic, typically accompanied by anomalous low pressure over the Barents Sea, enhanced wind speeds, and unstable boundary-layer conditions. While their analysis focused on ODEs, our findings highlight that BrO enhancement shows similar links to these meteorological situations. In addition, the strong positive correlation between BrO VMR profiles and aerosol extinction profiles (r = 0.58, p < 0.0001) indicates that atmospheric particles may play a key role in sustaining elevated BrO levels, either by serving as a direct source of reactive bromine or by recycling inactive bromine species through heterogeneous processes. The correlation with relative humidity (Fig. 7h) is very weak but positive (r = 0.10, p < 0.0001); the underlying causality, if any, remains unclear. Moving to the back-trajectory-based analysis, BrO shows a significant positive correlation with sea ice contact time (r = 0.48, p < 0.0001), whereas no significant correlation was found with open ocean contact (r = -0.02, p = 0.145). These results suggest that BrO observed in Ny-Ålesund during the spring of 2020 originated predominantly from sea ice regions. In Section 3.4, we further investigate the origins of reactive bromine air masses and quantify contributions from various sources, including firstyear and multi-year sea ice, snowpack emissions, open ocean, and free-tropospheric air.





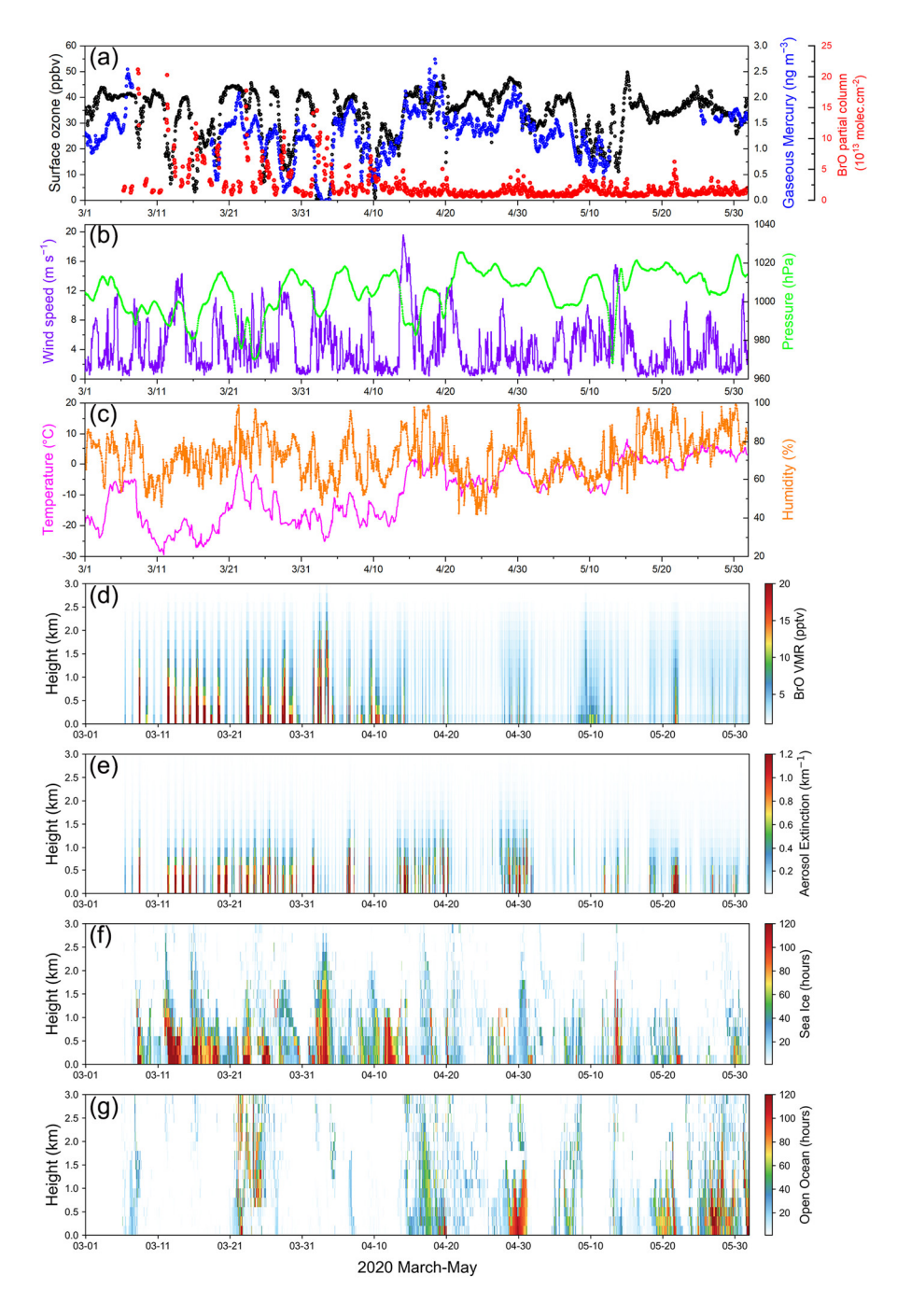


Figure 6. Panel (a) surface ozone (black dots), gaseous mercury (Hg(0)) (blue dots) and BrO partial column (red dots); (b) wind speed (purple line), pressure (green line); (c) temperature (pink line), relative humidity (orange line); (d) BrO profiles; (e) aerosol extinction profiles; (f) sea ice contact time (< 500 m) profiles along the 5-d backward trajectory; and (g) open ocean contact time (< 500 m) profiles along the 5-d backward trajectory between March and May 2020 in Ny-Ålesund.



385

390



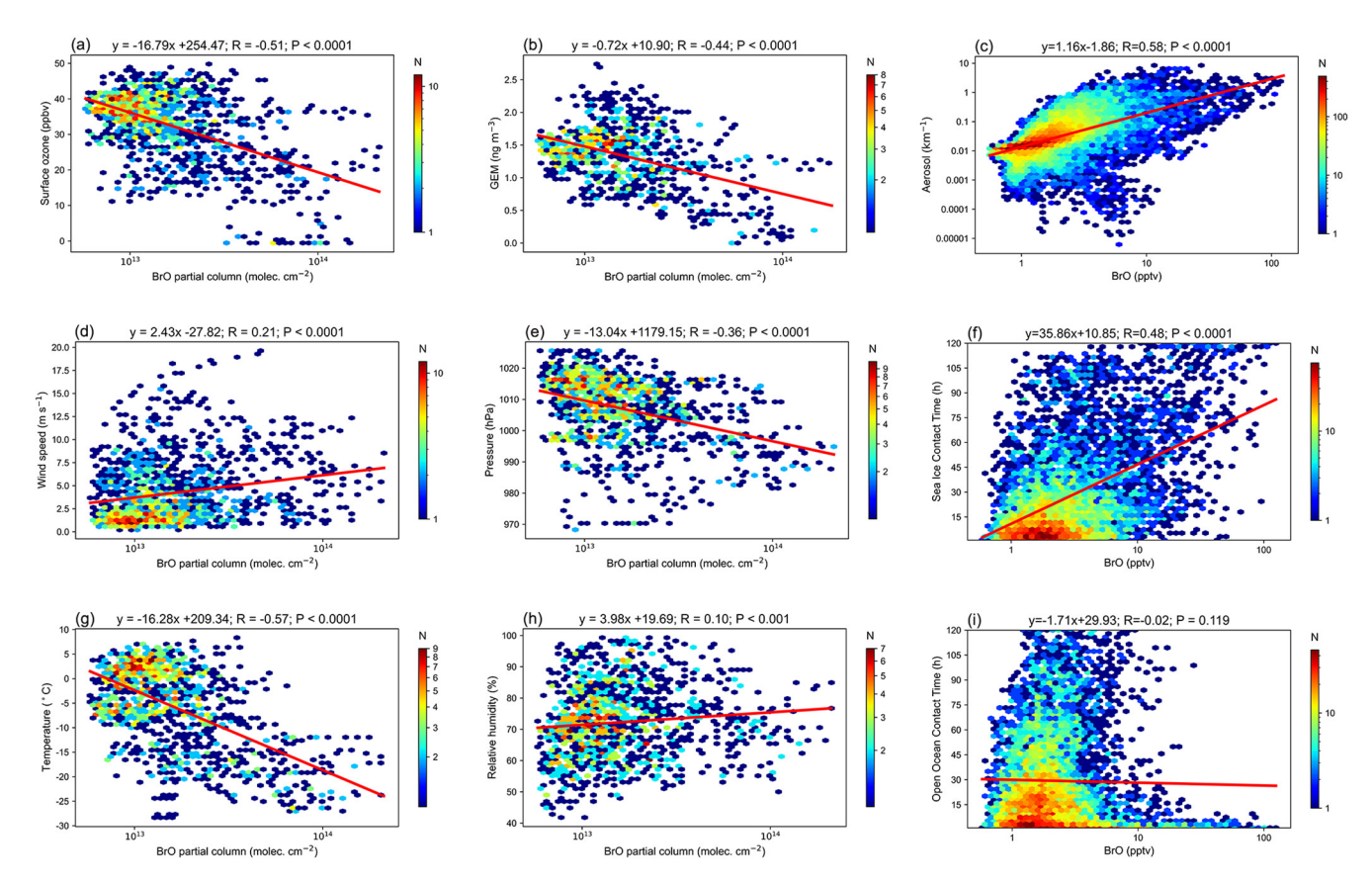


Figure 7. Correlation analysis between BrO and various parameters during March–May 2020. BrO partial column correlations are shown for surface ozone (a), GEM (b), wind speed (d), pressure (e), temperature (g), and relative humidity (h). BrO VMR profile correlations are shown for aerosol profiles (c), sea ice contact time (f), and open ocean contact time (i).

3.3.2 Comparison with p-TOMCAT results

The hourly MAX-DOAS BrO partial columns and p-TOMCAT BrO partial columns from March to May 2020 are presented in Fig. 8a. Overall, the MAX-DOAS BrO partial columns show good agreement with the p-TOMCAT BrO partial columns, with a correlation coefficient of 0.65 (p < 0.0001) in 2020 (Fig. 8b). During BEEs, p-TOMCAT generally captures the enhancement of BrO, coinciding with the occurrence of ODEs. The modelled BrO partial columns are, on average, approximately 60% higher than the MAX-DOAS BrO partial columns, which is in line with Yang et al. (2020), who reported that p-TOMCAT simulated BrO tropospheric columns during BEEs were about twice as high as observations. This discrepancy could be attributed to using the entire snowpack salinity, rather than the surface layer salinity, in the SSA parameterization, as bromine release from blowing-snow-sourced SSA responds almost linearly to snow salinity. Another factor that may have influenced bromine emissions is snow age. For instance, increasing the snow age from 1.5 d to 3 d is estimated to reduce BrO loading by approximately 30%. Other processes could also affect bromine chemistry, including the form of emitted reactive



400



bromine. Following our previous modelling setups, we assumed that all emitted bromine was in the form of Br₂; however, measurements have shown that it could also be BrCl (Buys et al., 2013; Pratt et al., 2013). In addition to chemical processes, model dynamical processes—such as the representation of the polar boundary layer—could also significantly influence near-surface BrO and ozone simulations (Yang et al., 2020).

Figure 8c presents the hourly surface ozone observations at the Zeppelin station, the corresponding p-TOMCAT ozone at the station height, and the ozone values of the model's lowest layer from March to May 2020. As shown in Fig. 8d, the p-TOMCAT ozone for 2020 is significantly correlated with the ozone observations (r = 0.53, p < 0.0001), and the model successfully captured major ODEs, such as those on March 28–29 and April 2–4, 2020. However, for short-term ODEs lasting less than one day—such as those on March 12, 16, and 25—the model fails to capture them accurately. This limitation is likely due to the coarse model resolution, which tends to overlook small-scale events (Yang et al., 2020).

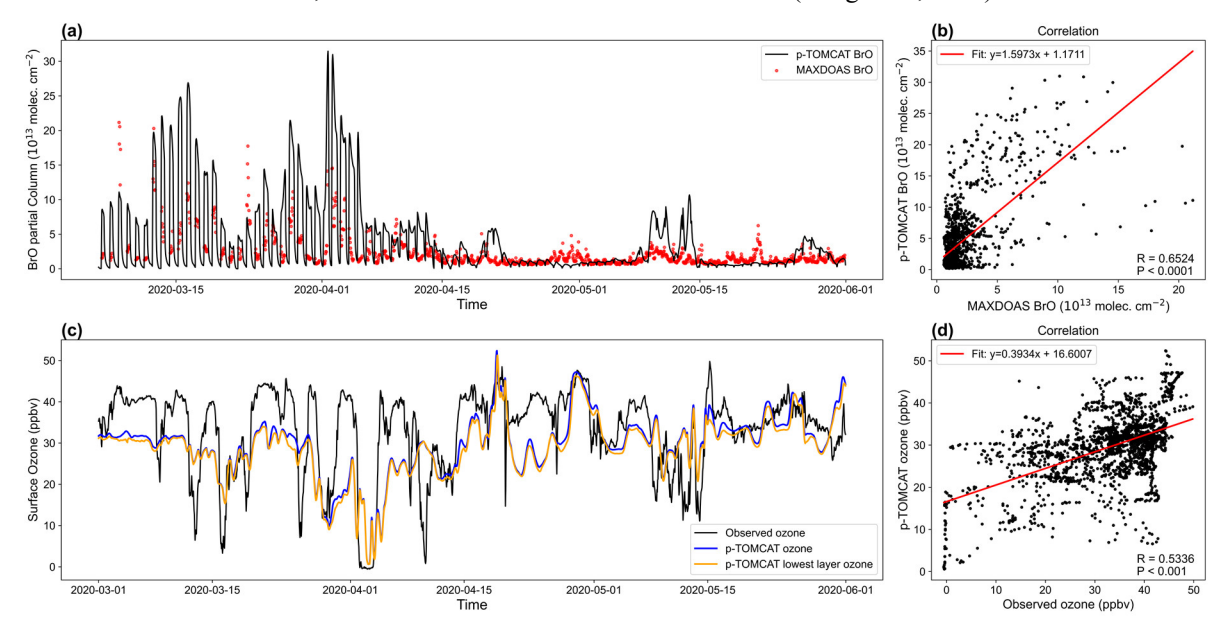


Figure 8. Time series of MAX-DOAS (red dots) and p-TOMCAT (black line) BrO partial columns in Ny-Ålesund from March to May 2020 (a), and their correlation with a line fit function (b). Time series of observed surface ozone (black line) at the Zeppelin station (474 m altitude) and p-TOMCAT ozone (blue line) at the corresponding altitude, as well as ozone in the lowest model layer (orange line) (c). (d) shows the correlation between the observations and the corresponding ozone with a line fit function.

3.4 Source analysis of BrO

3.4.1 Origins of air mass during BEEs and non-BEEs

Figure 9 illustrates the proportion of air mass contact time with different surface types (< 500 m) along the 5-day backward trajectories of air masses during BEEs and non-BEEs in Ny-Ålesund. Air masses located above 500 m were classified as belonging to the free troposphere. From March to May, air masses associated with BEEs exhibited the highest contact time



415

420

425

430

435

440

445



with sea ice, accounting for approximately half of the total time (54.7% in March, 50.9% in April, and 48.8% in May; see Table S1). The free troposphere represented about one-third of the total time (34.9%). When the boundary layer height was set to 1000 m, the proportion of free troposphere contact time decreased substantially to ~15%, while the sea ice contact time increased to 65.9% (see Table S2). Throughout March to May, the contact time of BEE-related air masses with the open ocean and land remained low, at approximately 6.8% and 6.3%, respectively, indicating that BEEs in Ny-Ålesund were primarily influenced by sea ice. In contrast, about 80% of non-BEE-related air masses were located in the free troposphere, with relatively low contact times with open ocean and sea ice over the same period.

To investigate the sources of reactive bromine in Ny-Ålesund, we followed the approach used in previous studies to determine air mass origins from the back-trajectory outputs of the HYSPLIT model (Pernov et al., 2024; Frieß et al., 2023). If any hourly trajectory point of an air mass associated with a BEE was located below 500 m, that point was included in the analysis. For each specific month, the total number of hourly trajectory points in each 1° × 1° surface grid was divided by the total number of hourly trajectory points in all grids during the three-month period (March-May), yielding the trajectory frequency distributions for each month during BEE events (Fig. 10d-f). The same procedure was applied to non-BEE events, with the results shown in Fig. 10g-i. To highlight the underlying land types, the monthly median distributions of sea ice age for March to May are shown in Fig. 10a-c. During BEEs, more than half of the air mass contact time within the boundary layer was associated with multi-year sea ice, with air masses mainly originating from multi-year rather than first-year sea ice (e.g., 56.1% vs. 23.8%; Fig. S3). During non-BEEs, over 30% of the contact time was still associated with multi-year sea ice (Fig. S3). Air masses within the boundary layer along the backward trajectories during BEEs primarily contacted northern sea ice, with more than two-thirds of the sea ice contact time linked to multi-year ice and only one-third to first-year ice (Fig. S3). The fractions of multi-year and first-year sea ice contact within the total sea ice contact time did not change substantially during non-BEEs (Fig. S3). In contrast, during non-BEEs, the percentage of air mass contact time (below 500 m) with open ocean increased significantly, rising from 10.5% during BEEs to 35.5% (Fig. S3). These results indicate that, throughout spring, reactive bromine arriving in Ny-Ålesund was primarily influenced by multi-year sea ice rather than younger ice, suggesting that multiyear sea ice may serve as a significant source of reactive bromine in the region.

Ny-Ålesund is located in a valley, which typically channels the local winds into northwesterly and southeasterly directions. Figure S4 shows the wind distribution measured in Ny-Ålesund from March to May during 2017–2023 for BEE and non-BEE periods. During BEEs, the wind rose exhibits a bimodal distribution, with nearly 50% of the time associated with northwesterly winds (270°–360°) and approximately 30% with southeasterly winds (90°–180°). Compared to southeasterly winds, northwesterly winds are associated with a higher proportion of strong winds. For BEEs, the 5-day backward trajectories of air masses arriving from the northwest show an average contact with sea ice of ~60% and with open ocean of less than 5%, while air masses from the southeast also exhibit a substantial sea ice contact of ~40% and an average open ocean contact of ~10%. In contrast, during non-BEE periods, more than half of the time is dominated by southeasterly winds, with only ~20% coming from the northwest, and the average contacts of these air masses with sea ice and open ocean are both less than 10%, which



455

460



may explain the absence of BEEs. These results further support that BEEs in Ny-Ålesund were primarily influenced by sea ice.

It should be noted that our analysis focuses only on influences within the latest 5 days. In a recent study, Yang et al. (2024) reported a longer lifetime of atmospheric reactive bromine as a family of approximately 17–42 days, which is significantly longer than the 4–10 days suggestion in their earlier studies (von Glasow et al., 2004; Yang et al., 2005). The potential contribution of air masses beyond 5 days is not considered in this study; and the accuracy of backward trajectories decreases significantly for periods longer than 5 days (Humphries et al., 2016; Rößler et al., 2018). To assess the sensitivity of our results, we repeated the calculation with a longer lifetime of 30 days. Minor changes are found in correlations between BrO and the cumulative bromine emission fluxes when the longer 30-day lifetime was used compared to 5 days, e.g. from values of r = 0.17-0.34 (5 days) to 0.15-0.30 (30 days) in the blowing snow flux calculation, and from r = 0.21-0.29 (5 days) to 0.18-0.26 (30 days) in the snowpack flux calculation under high wind speeds, see the section below for details.

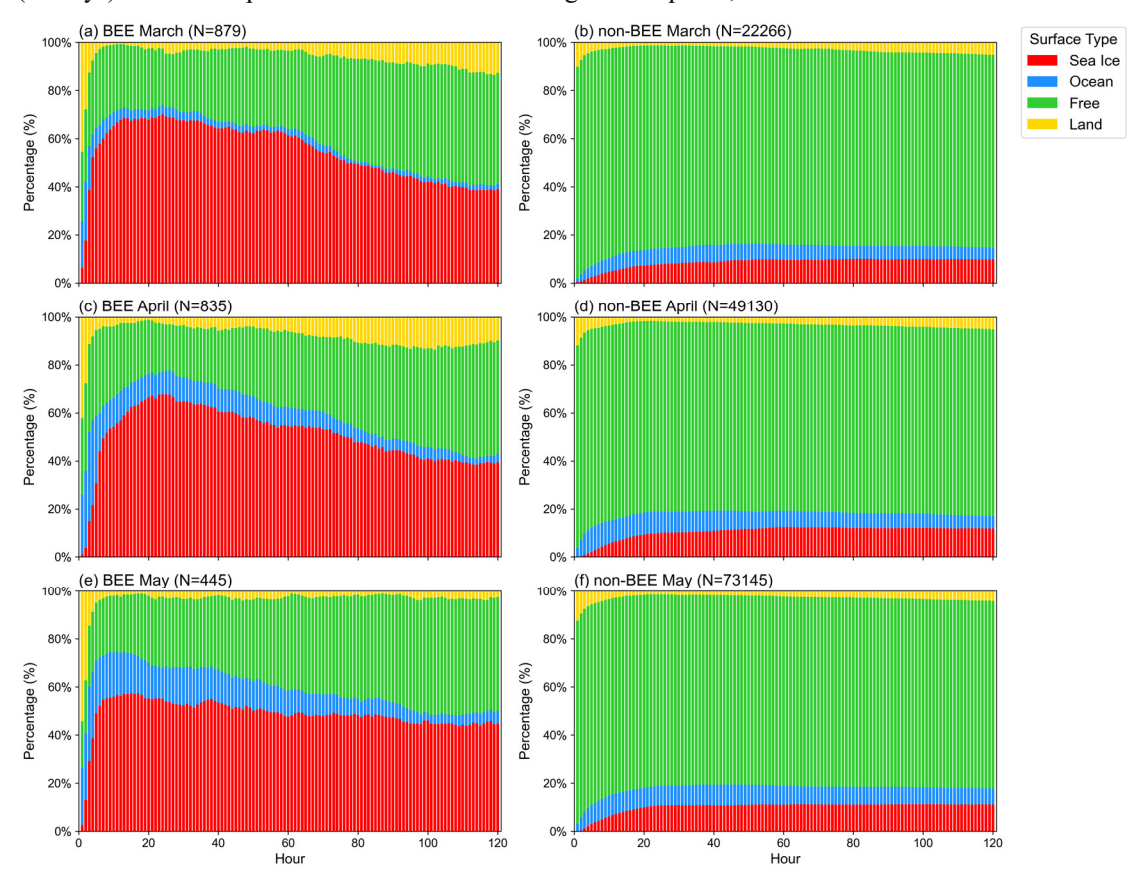


Figure 9. Percentage of air mass contact times with sea ice, open ocean, free troposphere and land along the 5-d backward trajectories during the identified BEEs and non-BEEs in Ny-Ålesund in March (a, b), April (c, d), and May(e, f) for the period of 2017 to 2023. The number N in each panel represents the monthly cumulative total of hours for air mass in each 200 m altitude interval within the 0-3 km range.





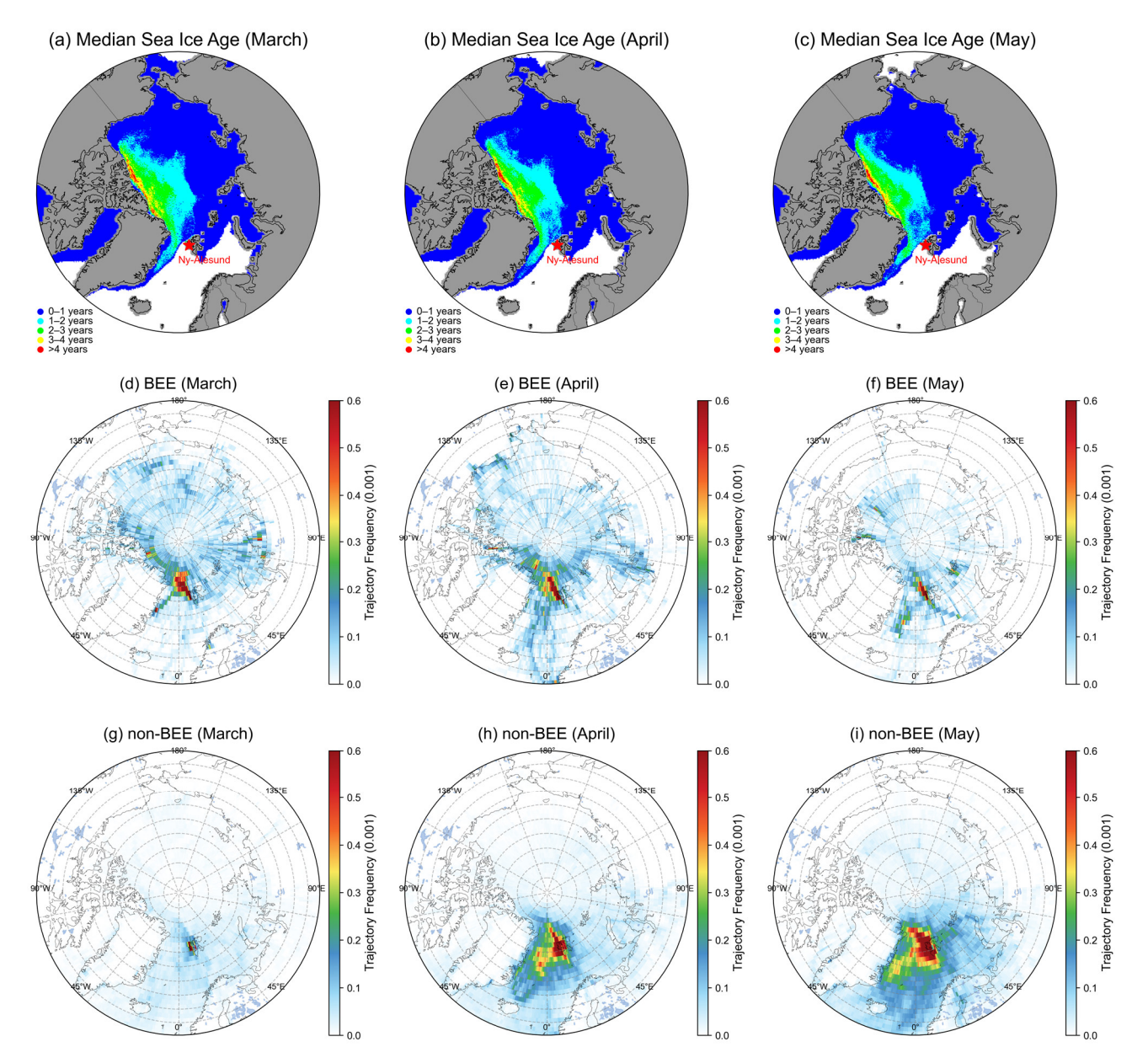


Figure 10. Monthly median sea ice age (a-c) and the frequency of air masses along the 5-d backward trajectories when the air masses are below 500 m during BEEs (d-f) and non-BEEs (g-i) in Ny-Ålesund for March, April, and May during 2017–2023.

3.4.2 Relationships with sea ice

465

Correlation analyses were performed among BrO VMR (0-3 km), aerosol extinction profiles, contact times over various surface types, and the corresponding bromine emission fluxes calculated from snowpack and SSA over the open ocean and



470

475

480

485

490

495



blowing snow. The variables used in these analyses are detailed in Table 2. Pearson correlation coefficients (PCC) were calculated to quantify these relationships (Fig. 11). The most notable finding is that aerosol extinction exhibits the strongest correlation with BrO among all variables, with r values ranging from 0.51 to 0.76 (p < 0.0001) from March to May, indicating a close association between airborne particles and the enhancement of reactive bromine in Ny-Ålesund.

BrO is positively correlated with the contact time of air masses with sea ice, with r ranging from 0.18 to 0.35 (p < 0.0001). Similarly, the cumulative bromine emission flux, calculated from blowing snow along the back-trajectories, also exhibits a positive correlation with BrO, with r ranging from 0.17 to 0.34 (p < 0.0001). In addition, two further analyses were conducted by segregating sea ice contact time according to wind speed: one for wind speeds ≤ 7 m s⁻¹ and another for wind speeds ≥ 7 m s⁻¹. The correlation analysis revealed that the r values under high wind speed conditions range from 0.26 to 0.42 (p < 0.0001), and are higher than the values of 0.10 to 0.19 (p < 0.0001) observed under low wind speed conditions (Fig. S5). These results suggest that strong winds favour reactive bromine release, with one proposed mechanism being SSA production from blowing snow (Yang et al., 2008; 2019). The small positive correlation coefficients under low wind speeds appear to support snowpack-based bromine emissions via photochemical processes. However, this could also be explained by the retention of reactive bromine in the near-surface layer following the cessation of blowing snow events.

To further investigate this mechanism, we analyzed the correlations between BrO, aerosol extinction, and modelled SSA mass concentrations from the p-TOMCAT model. BrO is significantly correlated with modelled blowing-snow-sourced SSA (Ssa_si) at Ny-Ålesund, with r ranging from 0.23 to 0.40 (p < 0.0001). When open-ocean-derived SSA is included, the correlation coefficients increase to 0.37–0.45 (p < 0.0001), providing strong support for SSA as a direct source of reactive bromine. Moreover, aerosol extinction retrieved from MAX-DOAS exhibits a notable positive correlation with modelled blowing-snow-sourced SSA in March (r = 0.26, p < 0.0001). However, this correlation becomes negative in April (r = -0.09) and May (r = -0.14), which may be attributed to enhanced transport of non-sea-salt aerosols from lower latitudes and increased biological activity along with strengthened vertical mixing within the lower troposphere during these months (Xian et al., 2022; Ji et al., 2025).

BrO is positively correlated with both first-year sea ice and multi-year sea ice from March to May. However, the correlation coefficients between BrO and the contact time with multi-year sea ice (0.17-0.29, p < 0.0001) are generally higher than those with first-year sea ice (0.03-0.23, p < 0.0001). These results are consistent with the back-trajectory findings presented in Section 3.4.1, highlighting the potential importance of multi-year sea ice in contributing to reactive bromine in Ny-Ålesund.





Table 2. Variables considered in the correlation analysis. BrO, Aer, F_{br} , F_{br

Variable	Description	
BrO	BrO VMR Profile retrieved from MAX-DOAS	
Aer	Aerosol extinction profile retrieved from MAX-DOAS	
F_{br}	Bromine flux from SSA over sea ice (Yang et al., 2008) and open ocean (Jaeglé et al., 2011	
F_{br_si}	Bromine flux from blowing snow SSA over sea ice	
F_{br_oo}	Bromine flux from open ocean sea spray	
Free	Contact time with free troposphere (> 500 m)	
Land	Contact time with land	
Ocean	Contact time with open ocean	
Seaice	Contact time with sea ice including first-year and multi-year ice	
$Seaice_ \leq 7 \text{ m s}^{-1}$	Contact time with sea ice at wind speed $\leq 7 \text{ m s}^{-1}$	
$Seaice_ > 7 \text{ m s}^{-1}$	Contact time with sea ice at wind speed $> 7 \text{ m s}^{-1}$	
FYI	Contact time with first-year sea ice	
MYI	Contact time with multi-year sea ice	
Seaice + Ocean	Contact time with sea ice and open ocean	
$F_{br_snow_FYI}$	Bromine flux from snowpack on first-year sea ice (Toyota et al., 2011)	
Fbr_snow_Seaice	Bromine flux from snowpack on total sea ice	
$F_{br_snow_} \leq 7~\text{m s}^{\scriptscriptstyle -1}$	Bromine flux from snowpack on sea ice at wind speed $\leq 7 \text{ m s}^{-1}$	
$F_{br_snow_} > 7~m~s^{-1}$	Bromine flux from snowpack on sea ice at wind speed $> 7 \text{ m s}^{-1}$	
Ssa_si	Modelled local SSA mass concentration from blowing snow over sea ice	
Ssa_oo	Modelled local SSA mass concentration from open ocean	
Ssa	Modelled local SSA mass concentration from sea ice and open ocean	

505 3.4.3 Relationship with open ocean, land and free troposphere

Previous studies have identified the open ocean as a potential source of reactive bromine (Sander et al., 2003). In this study, the correlation between BrO and the contact time of air masses with the open ocean is generally weak or negative, with r ranging from -0.13 to 0.07 (Fig. 11). Similarly, no significant correlation was found between BrO and the cumulative bromine emission flux calculated from the open ocean (r = -0.09 to 0.04). This is primarily due to the relatively small proportion of air masses (< 10% of total trajectory time from March to May; Table S1) that contacted the open ocean during BEEs. An exception occurred in May 2017, when the proportion of air mass contact time with the open ocean increased markedly to 37%. This





enhanced contact corresponded to a notable positive correlation between BrO and open-ocean contact time (r = 0.19, p < 0.0001), as well as between BrO and the cumulative bromine emission flux from the open ocean (r = 0.23, p < 0.0001).

From March to May, BrO is negatively or negligibly correlated with the contact time of air masses with land, with r ranging from 0.00 to -0.10. In contrast, BrO exhibits significant negative correlations with the contact time of air masses with the free troposphere, with r ranging from -0.29 to -0.40 (p < 0.0001). These results indicate that neither the free troposphere nor land served as sources of reactive bromine, and that increased air mass influence from the free troposphere may have reduced atmospheric BrO levels.

3.4.4 Relationship with snowpack-sourced bromine

In addition to SSA, snowpack on sea ice has been proposed as reactive bromine source, and this mechanism was examined in this study. Using the parameterization scheme of Toyota et al. (2011), cumulative snowpack bromine emissions were calculated along 5-day back-trajectories from March to May on first-year sea ice (denoted as F_{br_snow_FYI}) and on total sea ice (denoted as F_{br_snow_Seaice}), and these were directly compared with retrieved BrO. The results (Fig. 11) show that BrO exhibits no correlation with F_{br_snow_FYI} (r = 0.00–0.10). However, when both first-year and multi-year sea ice are included (i.e., F_{br_snow_Seaice}), a positive correlation emerges, with r values of 0.11–0.26 (p < 0.0001), indicating the importance of multi-year sea ice. Under low wind speed conditions (≤ 7 m s⁻¹, denoted as F_{br_snow_≤ 7 m s⁻¹), the correlation between BrO and cumulative snowpack bromine flux remains weak (r = 0.04–0.16). In contrast, under high wind speed conditions (F_{br_snow_> 7 m s⁻¹), the correlation is stronger (r = 0.21–0.29, p < 0.0001), suggesting that snowpack-related bromine emissions may be enhanced by high wind speeds.}}





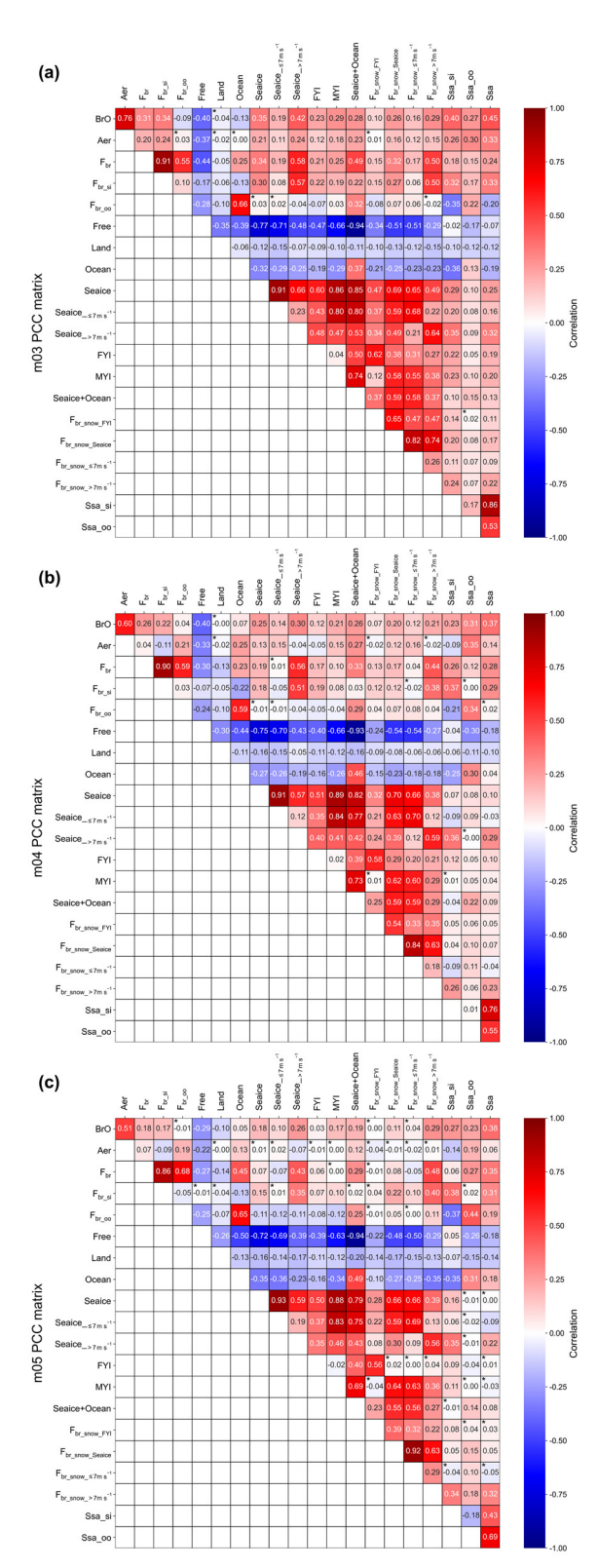






Figure 11. Pearson correlation matrix of MAX-DOAS BrO VMR and related variables in Ny-Ålesund for March (a), April (b), and May (c), based on data from 2017–2023 (2017–2022 for Ssa_si, Ssa_oo, and Ssa). Note that Ssa_si, Ssa_oo, and Ssa are local variables, rather than accumulated values along the 5-d backward trajectories. Descriptions of the variables are provided in Table 2. An asterisk (*) indicates cases where the relations are not significant at p-value (of the Pearson correlation) ≥ 0.0001.

535 4 Summary

540

545

550

555

560

In this study, we integrated seven years (2017–2023) of MAX-DOAS BrO observations in Ny-Ålesund with GOME-2B measurements, p-TOMCAT simulations, meteorological data, and HYSPLIT backward trajectories to analyze the sources and variability of tropospheric BrO from March to May during polar spring. The MAX-DOAS BrO partial columns (0–4 km) show strong agreement with overpassing GOME-2B tropospheric columns within 45 km. The mean monthly BrO partial column exhibits a decreasing trend from March to May (1.97 × 10^{11} molecules cm⁻² d⁻¹) with pronounced interannual variability. The most substantial short-term perturbations occur in March. Episodes of enhanced BrO frequently coincide with ODEs, highlighting the role of reactive bromine in Arctic atmospheric chemistry during spring.

Strong correlations between MAX-DOAS-retrieved BrO and aerosol extinction were observed, indicating a potential link between enhanced airborne particles and reactive bromine release at Ny-Ålesund. Backward trajectory analyses further revealed that enhanced BrO during BEEs is positively correlated with total sea ice contact time. Notably, the correlation coefficients between BrO and sea ice contact time are substantially larger (0.26–0.42) under high wind speed conditions (> 7 m s⁻¹) than under low wind speed conditions (0.10–0.19, \leq 7 m s⁻¹). These results suggest that strong winds enhance reactive bromine release from the sea ice surface, likely through the production of SSA from blowing snow, as previously proposed. This interpretation is further supported by the significant correlations between p-TOMCAT modelled SSA and retrieved BrO from March to May.

From March to May, BrO exhibits generally weak or negative correlations with air mass contact time with the open ocean and with the calculated bromine emission flux from sea spray. Weak or no correlations were also found with land contact time. These results indicate that neither the open ocean nor land serves as a major source of reactive bromine in Ny-Ålesund during spring. This can be explained by the fact that, during BEEs, total sea ice contact accounts for more than 50% of air mass contact time, whereas open ocean contact accounts for less than 10%, suggesting that sea ice surface processes dominate reactive bromine release.

Another finding from this study is that, during BEEs, more than half of the air masses within the boundary layer originate from regions covered by multi-year sea ice, particularly areas north of Greenland and the Canadian Arctic Archipelago. This may be attributed to Svalbard's geographic location, which allows a large proportion of air masses approaching Ny-Ålesund to pass over the major multi-year sea ice body in the Arctic, providing a substantial source of reactive bromine.

However, we could not rule out snowpack emissions as a reactive bromine source, given the positive correlations between BrO and both sea ice contact time and the calculated reactive bromine flux from snowpack, as parameterized. Under high wind

https://doi.org/10.5194/egusphere-2025-4601 Preprint. Discussion started: 18 November 2025

© Author(s) 2025. CC BY 4.0 License.



565

EGUsphere Preprint repository

speed conditions, the correlation coefficients increase markedly compared with calm conditions, underscoring the dynamical influence on reactive bromine release. Nevertheless, it remains unclear whether this enhancement results from the so-called "air-pumping" effect (Toyota et al., 2011) or from SSA production via blowing snow (Yang et al., 2008). These findings highlight the need for quantitative measurements of snowpack emissions over sea ice, together with polar boundary layer bromine budget analyses (Yang et al., 2024), to improve understanding of the relevant processes, accurately simulate polar springtime BEEs and ODEs, and assess their climate impacts through effects on atmospheric oxidizing capacity.

Data availability. Surface ozone and GEM observations at the Zeppelin station are available from the EBAS database (https://ebas-data.nilu.no/). Meteorological data from the atmospheric observatory in Ny-Ålesund are provided by AWI-Potsdam and accessed via the PANGAEA database (e.g., https://doi.org/10.1594/PANGAEA.914808). Sea ice age data are available from the NSIDC (https://daacdata.apps.nsidc.org/pub/DATASETS/nsidc0611_seaice_age_v4/). The MAX-DOAS BrO and aerosol profiles, GOME-2 tropospheric BrO column data, and p-TOMCAT simulation results in Ny-Ålesund will be available from the UK Polar Data Centre.

Author contribution. QL was responsible for data analysis, interpretation, and writing the original draft. YL provided funding support, contributed to data analysis, interpretation, and participated in manuscript review and editing. XY provided p-TOMCAT model results, contributed to data analysis, interpretation, and participated in manuscript review and editing. BZ and AR provided the GOME-2B satellite data, and AR also participated in manuscript review and editing. KD, HZ and KZ were responsible for the operation and maintenance of the MAX-DOAS instrument. FS contributed to resource provision and project management. WL supervised the overall research. QL prepared the initial draft of the manuscript with contributions from all co-authors.

Competing interests. Andreas Richter is a member of the editorial board of Atmospheric Chemistry and Physics, and the authors also have no other competing interests to declare.

Acknowledgement. We gratefully acknowledge the Polar Research Institute of China, and the Chinese Arctic Yellow River

Station for their support. We acknowledge the NASA NSIDC for providing sea ice information. Meteorological data were obtained from the PANGAEA database, and ERA5 reanalysis data were provided by the ECMWF. Surface ozone and GEM data were accessed from the EBAS database, which is managed by NILU. We thank BIRA for providing the QDOAS analysis





software. We also gratefully acknowledge the NOAA Air Resources Laboratory (ARL) for the provision of the HYSPLIT transport model used in this study.

Financial support. This research was financially supported by the National Natural Science Foundation of China (Grant Nos.41941011 and 41676184), the Youth Innovation Promotion Association of CAS (Grant No.2020439) and the Hefei Institutes of Physical Science Director's Fund (Grant number: BJPY2023B01). This work has received support from the NERC National Capability International grant SURface FluxEs In AnTarctica (SURFEIT): NE/X009319/1. A. Richter and B. Zilker acknowledge support by the Deutsche Forschungsgemeinschaft (DFG, German Research Foundation) project no. 268020496 TRR 172, within the Transregional Collaborative Research Center "ArctiC Amplification: Climate Relevant Atmospheric and SurfaCe Processes, and Feedback Mechanisms (AC)³".

References

600

- Abbatt, J. P. D., Thomas, J. L., Abrahamsson, K., Boxe, C., Granfors, A., Jones, A. E., King, M. D., Saiz-Lopez, A., Shepson, P. B., Sodeau, J., Toohey, D. W., Toubin, C., von Glasow, R., Wren, S. N., and Yang, X.: Halogen activation via interactions with environmental ice and snow in the polar lower troposphere and other regions, Atmospheric Chemistry and Physics, 12, 6237–6271, https://doi.org/10.5194/acp-12-6237-2012, 2012.
- Angot, H., Dastoor, A., De Simone, F., Gårdfeldt, K., Gencarelli, C. N., Hedgecock, I. M., Langer, S., Magand, O., Mastromonaco, M. N., Nordstrøm, C., Pfaffhuber, K. A., Pirrone, N., Ryjkov, A., Selin, N. E., Skov, H., Song, S., Sprovieri, F., Steffen, A., Toyota, K., Travnikov, O., Yang, X., and Dommergue, A.: Chemical cycling and deposition of atmospheric mercury in polar regions: review of recent measurements and comparison with models, Atmospheric Chemistry and Physics, 16, 10735–10763, https://doi.org/10.5194/acp-16-10735-2016, 2016.
- Barrie, L. and Platt, U.: Arctic tropospheric chemistry: An overview, Tellus B, 49, 450–454, https://doi.org/10.3402/tellusb.v49i5.15984, 1997.
- Barrie, L., Bottenheim, J., Schnell, R. C., Crutzen, P. J., and Rasmussen, R.: Ozone destruction and photochemical reactions at Polar sunrise in the lower Arctic atmosphere, Nature, 334, 138–141, 1988.
 - Begoin, M., Richter, A., Weber, M., Kaleschke, L., Tian-Kunze, X., Stohl, A., Theys, N., and Burrows, J. P.: Satellite observations of long range transport of a large BrO plume in the Arctic, Atmospheric Chemistry and Physics, 10, 6515–6526, https://doi.org/10.5194/acp-10-6515-2010, 2010.
- Benavent, N., Mahajan, A. S., Li, Q., Cuevas, C. A., Schmale, J., Angot, H., Jokinen, T., Quéléver, L. L. J., Blechschmidt, A.M., Zilker, B., Richter, A., Serna, J. A., Garcia-Nieto, D., Fernandez, R. P., Skov, H., Dumitrascu, A., Simões Pereira, P.,
 Abrahamsson, K., Bucci, S., Duetsch, M., Stohl, A., Beck, I., Laurila, T., Blomquist, B., Howard, D., Archer, S. D.,
 Bariteau, L., Helmig, D., Hueber, J., Jacobi, H.-W., Posman, K., Dada, L., Daellenbach, K. R., and Saiz-Lopez, A.:



625

630

5, 2003.



- Substantial contribution of iodine to Arctic ozone destruction, Nature Geoscience, 15, 770–773, https://doi.org/10.1038/s41561-022-01018-w, 2022.
- Bocquet, M., Fleury, S., Rémy, F., and Piras, F.: Arctic and Antarctic Sea Ice Thickness and Volume Changes From Observations Between 1994 and 2023, Journal of Geophysical Research: Oceans, 129, e2023JC020848, https://doi.org/10.1029/2023jc020848, 2024.
 - Bognar, K., Zhao, X., Strong, K., Chang, R. Y. W., Frieß, U., Hayes, P. L., McClure-Begley, A., Morris, S., Tremblay, S., and Vicente-Luis, A.: Measurements of Tropospheric Bromine Monoxide Over Four Halogen Activation Seasons in the Canadian High Arctic, Journal of Geophysical Research: Atmospheres, 125, e2020JD033015, https://doi.org/10.1029/2020jd033015, 2020.
 - Bogumil, K., Orphal, J., Homann, T., Voigt, S., Spietz, P., Fleischmann, O. C., Vogel, A., Hartmann, M., Kromminga, H., Bovensmann, H., Frerick, J., and Burrows, J. P.: Measurements of molecular absorption spectra with the SCIAMACHY pre-flight model: instrument characterization and reference data for atmospheric remote-sensing in the 230–2380 nm region, Journal of Photochemistry and Photobiology A: Chemistry, 157, 167–184, https://doi.org/10.1016/s1010-6030(03)00062-
 - Bottenheim, J. W., Gallant, A. G., and Brice, K. A.: Measurements of NO_y species and O₃ at 82°N latitude, Geophys. Res. Lett., 13, 113–116, 1986.
- Bougoudis, I., Blechschmidt, A.-M., Richter, A., Seo, S., Burrows, J. P., Theys, N., and Rinke, A.: Long-term time series of
 Arctic tropospheric BrO derived from UV–VIS satellite remote sensing and its relation to first-year sea ice, Atmospheric
 Chemistry and Physics, 20, 11869–11892, https://doi.org/10.5194/acp-20-11869-2020, 2020.
 - Brockway, N., Peterson, P. K., Bigge, K., Hajny, K. D., Shepson, P. B., Pratt, K. A., Fuentes, J. D., Starn, T., Kaeser, R., Stirm, B. H., and Simpson, W. R.: Tropospheric bromine monoxide vertical profiles retrieved across the Alaskan Arctic in springtime, Atmospheric Chemistry and Physics, 24, 23–40, https://doi.org/10.5194/acp-24-23-2024, 2024.
- 640 Brühl, C. and Crutzen, P. J.: MPIC two-dimensional model, in: The Atmospheric Effects of Stratospheric Aircraft, NASA Ref. Publ, 1292, 103–104, 1993.
 - Burd, J. A., Peterson, P. K., Nghiem, S. V., Perovich, D. K., and Simpson, W. R.: Snowmelt onset hinders bromine monoxide heterogeneous recycling in the Arctic, Journal of Geophysical Research: Atmospheres, 122, 8297–8309, https://doi.org/10.1002/2017jd026906, 2017.
- 645 Burrows, J. P., Platt, U., and Borrell, P. (Eds.): Tropospheric remote sensing from space, in: The remote sensing of tropospheric composition from space, Springer-Verlag, Berlin Heidelberg, 1–65, 2011.
 - Buys, Z., Brough, N., Huey, L. G., Tanner, D. J., von Glasow, R., and Jones, A. E.: High temporal resolution Br2, BrCl and BrO observations in coastal Antarctica, Atmos. Chem. Phys., 13, 1329–1343, https://doi.org/10.5194/acp-13-1329-2013, 2013.



655

660



- Cao, Y., Wang, Z., Liu, J., Ma, Q., Li, S., Liu, J., Li, H., Zhang, P., Chen, T., Wang, Y., Chu, B., Zhang, X., Saiz-Lopez, A., Francisco, J. S., and He, H.: Spontaneous Molecular Bromine Production in Sea-Salt Aerosols, Angew Chem Int Ed Engl, 63, e202409779, https://doi.org/10.1002/anie.202409779, 2024.
 - Chen, D., Luo, Y., Yang, X., Si, F., Dou, K., Zhou, H., Qian, Y., Hu, C., Liu, J., and Liu, W.: Study of an Arctic blowing snow-induced bromine explosion event in Ny-Alesund, Svalbard, Sci Total Environ, 839, 156335, https://doi.org/10.1016/j.scitotenv.2022.156335, 2022.
 - Choi, S., Theys, N., Salawitch, R. J., Wales, P. A., Joiner, J., Canty, T. P., Chance, K., Suleiman, R. M., Palm, S. P., Cullather, R. I., Darmenov, A. S., da Silva, A., Kurosu, T. P., Hendrick, F., and Van Roozendael, M.: Link Between Arctic Tropospheric BrO Explosion Observed From Space and Sea-Salt Aerosols From Blowing Snow Investigated Using Ozone Monitoring Instrument BrO Data and GEOS-5 Data Assimilation System, Journal of Geophysical Research: Atmospheres, 123, 6954–6983, https://doi.org/10.1029/2017jd026889, 2018.
 - Comiso, J. C., Meier, W. N., and Gersten, R.: Variability and trends in the Arctic Sea ice cover: Results from different techniques, Journal of Geophysical Research: Oceans, 122, 6883–6900, https://doi.org/10.1002/2017jc012768, 2017.
 - Criscitiello, A. S., Geldsetzer, T., Rhodes, R. H., Arienzo, M., McConnell, J., Chellman, N., Osman, M. B., Yackel, J. J., and Marshall, S.: Marine Aerosol Records of Arctic Sea-Ice and Polynya Variability From New Ellesmere and Devon Island Firn Cores, Nunavut, Canada, Journal of Geophysical Research: Oceans, 126, e2021JC017205, https://doi.org/10.1029/2021jc017205, 2021.
 - Custard, K. D., Raso, A. R. W., Shepson, P. B., Staebler, R. M., and Pratt, K. A.: Production and Release of Molecular Bromine and Chlorine from the Arctic Coastal Snowpack, ACS Earth and Space Chemistry, 1, 142–151, https://doi.org/10.1021/acsearthspacechem.7b00014, 2017.
- Danckaert, T., Fayt, C., Van Roozendael, M., De Smedt, I., Letocart, V., Merlaud, A., and Pinardi, G.: QDOAS Software user manual, Belgian Institute for Space Aeronomy (3.2 ed.) [Computer software manual], 2017.
 - Dukhovskoy, D. S., Ubnoske, J., Blanchard-Wrigglesworth, E., Hiester, H. R., and Proshutinsky, A.: Skill metrics for evaluation and comparison of sea ice models, Journal of Geophysical Research: Oceans, 120, 5910–5931, https://doi.org/10.1002/2015jc010989, 2015.
- 675 Engvall Stjernberg, A.-C., Skorokhod, A., Paris, J.-D., Elansky, N., Nédélec, P., and Stohl, A.: Low concentrations of near-surface ozone in Siberia, Tellus, 63, 011607, https://doi.org/10.3402/tellusb.v64i0.11607, 2011.
 - Errera, Q. and Fonteyn, D.: Four-dimensional variational chemical assimilation of CRISTA stratospheric measurements, Journal of Geophysical Research: Atmospheres, 106, 12253–12265, https://doi.org/10.1029/2001jd900010, 2001.
- Falk, S. and Sinnhuber, B.-M.: Polar boundary layer bromine explosion and ozone depletion events in the chemistry–climate model EMAC v2.52: implementation and evaluation of AirSnow algorithm, Geoscientific Model Development, 11, 1115–1131, https://doi.org/10.5194/gmd-11-1115-2018, 2018.
 - Fan, S.-M., and Jacob, D. J.: Surface ozone depletion in Arctic spring sustained by bromine reactions on aerosols, Nature, 359, 522–524, https://doi.org/10.1038/359522a0, 1992.





- Fleischmann, O. C., Hartmann, M., Burrows, J. P., and Orphal, J.: New ultraviolet absorption cross-sections of BrO at atmospheric temperatures measured by time-windowing Fourier transform spectroscopy, Journal of Photochemistry and Photobiology A: Chemistry, 168, 117–132, https://doi.org/10.1016/j.jphotochem.2004.03.026, 2004.
 - Frey, M. M., Norris, S. J., Brooks, I. M., Anderson, P. S., Nishimura, K., Yang, X., Jones, A. E., Nerentorp Mastromonaco, M. G., Jones, D. H., and Wolff, E. W.: First direct observation of sea salt aerosol production from blowing snow above sea ice, Atmos. Chem. Phys., 20, 2549–2578, https://doi.org/10.5194/acp-20-2549-2020, 2020.
- 690 Frieß, U., Hollwedel, J., König-Langlo, G., Wagner, T., and Platt, U.: Dynamics and chemistry of tropospheric bromine explosion events in the Antarctic coastal region, Journal of Geophysical Research: Atmospheres, 109, D06305, https://doi.org/10.1016/10.1029/2003jd004133, 2004.
 - Frieß, U., Monks, P. S., Remedios, J. J., Rozanov, A., Sinreich, R., Wagner, T., and Platt, U.: MAX-DOAS O4 measurements: A new technique to derive information on atmospheric aerosols: 2. Modeling studies, Journal of Geophysical Research: Atmospheres, 111, D14203, https://doi.org/10.1029/2005jd006618, 2006.
 - Frieß, U., Sihler, H., Sander, R., Pöhler, D., Yilmaz, S., and Platt, U.: The vertical distribution of BrO and aerosols in the Arctic: Measurements by active and passive differential optical absorption spectroscopy, Journal of Geophysical Research: Atmospheres, 116, D00R04, https://doi.org/10.1029/2011jd015938, 2011.
- Frieß, U., Kreher, K., Querel, R., Schmithüsen, H., Smale, D., Weller, R., and Platt, U.: Source mechanisms and transport patterns of tropospheric bromine monoxide: findings from long-term multi-axis differential optical absorption spectroscopy measurements at two Antarctic stations, Atmospheric Chemistry and Physics, 23, 3207–3232, https://doi.org/10.5194/acp-23-3207-2023, 2023.
- General, S., Pöhler, D., Sihler, H., Bobrowski, N., Frieß, U., Zielcke, J., Horbanski, M., Shepson, P. B., Stirm, B. H., Simpson, W. R., Weber, K., Fischer, C., and Platt, U.: The Heidelberg Airborne Imaging DOAS Instrument (HAIDI) a novel imaging DOAS device for 2-D and 3-D imaging of trace gases and aerosols, Atmospheric Measurement Techniques, 7, 3459–3485, https://doi.org/10.5194/amt-7-3459-2014, 2014.
 - Gong, S. L.: A parameterization of sea-salt aerosol source function for sub- and super-micron particles, Global Biogeochemical Cycles, 17, 1097, https://doi.org/10.1029/2003gb002079, 2003.
- Gong, X., Zhang, J., Croft, B., Yang, X., Frey, M. M., Bergner, N., Chang, R. Y.-W., Creamean, J. M., Kuang, C., Martin, R.
 V., Ranjithkumar, A., Sedlacek, A. J., Uin, J., Willmes, S., Zawadowicz, M. A., Pierce, J. R., Shupe, M. D., Schmale, J., and Wang, J.: Arctic warming by abundant fine sea salt aerosols from blowing snow, Nat. Geosci., 16, 768–774, https://doi.org/10.1038/s41561-023-01254-8, 2023.
- Halfacre, J. W., Knepp, T. N., Shepson, P. B., Thompson, C. R., Pratt, K. A., Li, B., Peterson, P. K., Walsh, S. J., Simpson, W. R., Matrai, P. A., Bottenheim, J. W., Netcheva, S., Perovich, D. K., and Richter, A.: Temporal and spatial characteristics of ozone depletion events from measurements in the Arctic, Atmospheric Chemistry and Physics, 14, 4875–4894, https://doi.org/10.5194/acp-14-4875-2014, 2014.



745



- Halfacre, J. W., Shepson, P. B., and Pratt, K. A.: pH-dependent production of molecular chlorine, bromine, and iodine from frozen saline surfaces, Atmospheric Chemistry and Physics, 19, 4917–4931, https://doi.org/10.5194/acp-19-4917-2019, 2019.
- Hausmann, M. and Platt, U.: Spectroscopic measurement of bromine oxide and ozone in the high Arctic during Polar Sunrise Experiment 1992, J. Geophys. Res., 99, 25399–25413, https://doi.org/10.1029/94JD01314, 1994.
 - Hersbach, H., Bell, B., Berrisford, P., Hirahara, S., Horányi, A., Muñoz-Sabater, J., Nicolas, J., Peubey, C., Radu, R., Schepers, D., Simmons, A., Soci, C., Abdalla, S., Abellan, X., Balsamo, G., Bechtold, P., Biavati, G., Bidlot, J., Bonavita, M., De Chiara, G., Dahlgren, P., Dee, D., Diamantakis, M., Dragani, R., Flemming, J., Forbes, R., Fuentes, M., Geer, A.,
- Haimberger, L., Healy, S., Hogan, R. J., Hólm, E., Janisková, M., Keeley, S., Laloyaux, P., Lopez, P., Lupu, C., Radnoti, G., de Rosnay, P., Rozum, I., Vamborg, F., Villaume, S., and Thépaut, J. N.: The ERA5 global reanalysis, Q. J. Roy. Meteor. Soc., 146, 1999–2049, https://doi.org/10.1002/qj.3803, 2020.
 - Hirdman, D., Aspmo, K., Burkhart, J. F., Eckhardt, S., Sodemann, H., and Stohl, A.: Transport of mercury in the Arctic atmosphere: Evidence for a spring-time net sink and summer-time source, Geophysical Research Letters, 36, L12814, https://doi.org/10.1029/2009gl038345, 2009.
 - Hönninger, G., Leser, H., Sebastián, O., and Platt, U.: Ground-based measurements of halogen oxides at the Hudson Bay by active longpath DOAS and passive MAX-DOAS, Geophysical Research Letters, 31, L04111, https://doi.org/10.1029/2003gl018982, 2004.
- Huang, J., Jaeglé, L., Chen, Q., Alexander, B., Sherwen, T., Evans, M. J., Theys, N., and Choi, S.: Evaluating the impact of blowing-snow sea salt aerosol on springtime BrO and O₃ in the Arctic, Atmospheric Chemistry and Physics, 20, 7335–7358, https://doi.org/10.5194/acp-20-7335-2020, 2020.
 - Humphries, R. S., Klekociuk, A. R., Schofield, R., Keywood, M., Ward, J., and Wilson, S. R.: Unexpectedly high ultrafine aerosol concentrations above East Antarctic sea ice, Atmos. Chem. Phys., 16, 2185–2206, https://doi.org/10.5194/acp-16-2185-2016, 2016.
- Jacobi, H. W., Kaleschke, L., Richter, A., Rozanov, A., and Burrows, J. P.: Observation of a fast ozone loss in the marginal ice zone of the Arctic Ocean, Journal of Geophysical Research: Atmospheres, 111, D15309, https://doi.org/10.1029/2005jd006715, 2006.
 - Jaeglé, L., Quinn, P. K., Bates, T. S., Alexander, B., and Lin, J.-T.: Global distribution of sea salt aerosols: new constraints from in situ and remote sensing observations, Atmos. Chem. Phys., 11, 3137–3157, https://doi.org/10.5194/acp-11-3137-2011, 2011.
 - Ji, D., Palm, M., Buschmann, M., Ebell, K., Maturilli, M., Sun, X., and Notholt, J.: Hygroscopic aerosols amplify longwave downward radiation in the Arctic, Atmos. Chem. Phys., 25, 3889–3904, https://doi.org/10.5194/acp-25-3889-2025, 2025.
 - Jones, A. E., Anderson, P. S., Wolff, E. W., Turner, J., Rankin, A. M., and Colwell, S. R.: A role for newly forming sea ice in springtime polar tropospheric ozone loss? Observational evidence from Halley station, Antarctica, Journal of Geophysical Research: Atmospheres, 111, D08306, https://doi.org/10.1029/2005jd006566, 2006.





- Jones, A. E., Anderson, P. S., Begoin, M., Brough, N., Hutterli, M. A., Marshall, G. J., Richter, A., Roscoe, H. K., and Wolff, E. W.: BrO, blizzards, and drivers of polar tropospheric ozone depletion events, Atmos. Chem. Phys., 9, 4639–4652, https://doi.org/10.5194/acp-9-4639-2009, 2009.
- Kaleschke, L., Richter, A., Burrows, J., Afe, O., Heygster, G., Notholt, J., Rankin, A. M., Roscoe, H. K., Hollwedel, J., Wagner,
 T., and Jacobi, H. W.: Frost flowers on sea ice as a source of sea salt and their influence on tropospheric halogen chemistry,
 Geophysical Research Letters, 31, L16114, https://doi.org/10.1029/2004gl020655, 2004.
 - Kirpes, R. M., Bonanno, D., May, N. W., Fraund, M., Barget, A. J., Moffet, R. C., Ault, A. P., and Pratt, K. A.: Wintertime Arctic Sea Spray Aerosol Composition Controlled by Sea Ice Lead Microbiology, ACS Cent Sci, 5, 1760–1767, https://doi.org/10.1021/acscentsci.9b00541, 2019.
- Kleist, D. T., Parrish, D. F., Derber, J. C., Treadon, R., Wu, W., and Lord, S.: Introduction of the GSI into the NCEP Global Data Assimilation System, Weather Forecast., 24, 1691–1705, https://doi.org/10.1175/2009WAF2222201.1, 2009.
 - Kromminga, H., Orphal, J., Spietz, P., Voigt, S., and Burrows, J. P.: New measurements of OClO absorption cross-sections in the 325–435 nm region and their temperature dependence between 213 and 293 K, Journal of Photochemistry and Photobiology A: Chemistry, 157, 149–160, https://doi.org/10.1016/s1010-6030(03)00071-6, 2003.
- Langendörfer, U., Lehrer, E., Wagenbach, D., and Platt, U.: Observation of filterable bromine variabilities during Arctic tropospheric ozone depletion events in high (1 hour) time resolution, J. Atmos. Chem., 34, 39–54, https://doi.org/10.1023/A:1006217001008, 1999.
 - Lehrer, E., Hönninger, G., and Platt, U.: A one dimensional model study of the mechanism of halogen liberation and vertical transport in the polar troposphere, Atmos. Chem. Phys., 4, 2427–2440, https://doi.org/10.5194/acp-4-2427-2004, 2004.
- Liao, J., Sihler, H., Huey, L. G., Neuman, J. A., Tanner, D. J., Friess, U., Platt, U., Flocke, F. M., Orlando, J. J., Shepson, P. B., Beine, H. J., Weinheimer, A. J., Sjostedt, S. J., Nowak, J. B., Knapp, D. J., Staebler, R. M., Zheng, W., Sander, R., Hall, S. R., and Ullmann, K.: A comparison of Arctic BrO measurements by chemical ionization mass spectrometry and long path-differential optical absorption spectroscopy, Journal of Geophysical Research: Atmospheres, 116, D00R02, https://doi.org/10.1029/2010jd014788, 2011.
- Liao, J., Huey, L. G., Tanner, D. J., Flocke, F. M., Orlando, J. J., Neuman, J. A., Nowak, J. B., Weinheimer, A. J., Hall, S. R., Smith, J. N., Fried, A., Staebler, R. M., Wang, Y., Koo, J. H., Cantrell, C. A., Weibring, P., Walega, J., Knapp, D. J., Shepson, P. B., and Stephens, C. R.: Observations of inorganic bromine (HOBr, BrO, and Br₂) speciation at Barrow, Alaska, in spring 2009, Journal of Geophysical Research: Atmospheres, 117, D00R16, https://doi.org/10.1029/2011jd016641, 2012.
- Lieb-Lappen, R. M. and Obbard, R. W.: The role of blowing snow in the activation of bromine over first-year Antarctic sea ice, Atmospheric Chemistry and Physics, 15, 7537–7545, https://doi.org/10.5194/acp-15-7537-2015, 2015.
 - Luo, Y., Si, F., Zhou, H., Dou, K., Liu, Y., and Liu, W.: Observations and source investigations of the boundary layer bromine monoxide (BrO) in the Ny-Ålesund Arctic, Atmospheric Chemistry and Physics, 18, 9789–9801, https://doi.org/10.5194/acp-18-9789-2018, 2018.



810



- Macfarlane, Amy R; Schneebeli, Martin; Dadic, Ruzica; Wagner, David N; Arndt, Stefanie; Clemens-Sewall, David; Hämmerle, Stefan; Hannula, Henna-Reetta; Jaggi, Matthias; Kolabutin, Nikolai; Krampe, Daniela; Lehning, Michael; Matero, Ilkka; Nicolaus, Marcel; Oggier, Marc; Pirazzini, Roberta; Polashenski, Chris; Raphael, Ian; Regnery, Julia; Shimanchuck, Egor; Smith, Madison M; Tavri, Aikaterini.: Snowpit raw data collected during the MOSAiC expedition [dataset bundled publication], PANGAEA, https://doi.org/10.1594/PANGAEA.935934, 2021.
- Macfarlane, AR, Schneebeli, M, Dadic, R, Tavri, A, Immerz, A, Polashenski, C, Krampe, D, Clem ens-Sewall, D, Wagner, DN, Perovich, DK, Henna-Reetta, H, Raphael, I, Matero, I, Regnery, J, Smith, MM, Nicolaus, M, Jaggi, M, Oggier, M, Webster, MA, Lehning, M, Kolabutin, N, Itkin, P, Naderpour, R, Pirazzini, R, Ha¨mmerle, S, Arndt, S, Fons, S.: A database of snow on sea ice in the central Arctic collected during the MOSAiC expedition. Scientific Data, 10, 398, http://dx.doi.org/10.1038/s41597-023-02273-1, 2023.
- Marelle, L., Thomas, J. L., Ahmed, S., Tuite, K., Stutz, J., Dommergue, A., Simpson, W. R., Frey, M. M., and Baladima, F.: Implementation and Impacts of Surface and Blowing Snow Sources of Arctic Bromine Activation Within WRF-Chem 4.1.1, J Adv Model Earth Syst, 13, e2020MS002391, https://doi.org/10.1029/2020MS002391, 2021.
- Maturilli, M.: Continuous meteorological observations at station Ny-Ålesund (2017-03), Alfred Wegener Institute Research Unit Potsdam, PANGAEA, https://doi.org/10.1594/PANGAEA.894597, 2018. (similar datasets for other years from 2017 to 2023 are available at PANGAEA)
 - Nghiem, S. V., Rigor, I. G., Richter, A., Burrows, J. P., Shepson, P. B., Bottenheim, J., Barber, D. G., Steffen, A., Latonas, J., Wang, F., Stern, G., Clemente-Colón, P., Martin, S., Hall, D. K., Kaleschke, L., Tackett, P., Neumann, G., and Asplin, M. G.: Field and satellite observations of the formation and distribution of Arctic atmospheric bromine above a rejuvenated sea ice cover, Journal of Geophysical Research: Atmospheres, 117, D00S05, https://doi.org/10.1029/2011jd016268, 2012.
- Obbard, R. W., Roscoe, H. K., Wolff, E. W., and Atkinson, H. M.: Frost flower surface area and chemistry as a function of salinity and temperature, Journal of Geophysical Research: Atmospheres, 114, D20305, https://doi.org/10.1029/2009jd012481, 2009.
 - Oltmans, S. J., and Komhyr, W. D.: Surface ozone distributions and variations from 1973–1984: Measurements at the NOAA Geophysical Monitoring for Climatic Change Baseline Observatories, Journal of Geophysical Research: Atmospheres, 91, 5229–5236, https://doi.org/10.1029/JD091iD04p05229, 1986.
 - Oum, K. W., Lakin, M. J., and Finlayson-Pitts, B. J.: Bromine activation in the troposphere by the dark reaction of O₃ with seawater ice, Geophysical Research Letters, 25, 3923–3926, https://doi.org/10.1029/1998g1900078, 1998.
 - Pernov, J. B., Hjorth, J. L., Sørensen, L. L., and Skov, H.: On the dynamics of ozone depletion events at Villum Research Station in the High Arctic, Atmospheric Chemistry and Physics, 24, 13603–13631, https://doi.org/10.5194/acp-24-13603-2024, 2024.
 - Peterson, P. K., Simpson, W. R., Pratt, K. A., Shepson, P. B., Frieß, U., Zielcke, J., Platt, U., Walsh, S. J., and Nghiem, S. V.: Dependence of the vertical distribution of bromine monoxide in the lower troposphere on meteorological factors such as



840



- wind speed and stability, Atmospheric Chemistry and Physics, 15, 2119–2137, https://doi.org/10.5194/acp-15-2119-2015, 2015.
- Peterson, P. K., Pöhler, D., Sihler, H., Zielcke, J., General, S., Frieß, U., Platt, U., Simpson, W. R., Nghiem, S. V., Shepson, P. B., Stirm, B. H., Dhaniyala, S., Wagner, T., Caulton, D. R., Fuentes, J. D., and Pratt, K. A.: Observations of bromine monoxide transport in the Arctic sustained on aerosol particles, Atmospheric Chemistry and Physics, 17, 7567–7579, https://doi.org/10.5194/acp-17-7567-2017, 2017.
- Peterson, P. K., Hartwig, M., May, N. W., Schwartz, E., Rigor, I., Ermold, W., Steele, M., Morison, J. H., Nghiem, S. V., and Pratt, K. A.: Snowpack measurements suggest role for multi-year sea ice regions in Arctic atmospheric bromine and chlorine chemistry, Elementa: Science of the Anthropocene, 7, 14, https://doi.org/10.1525/elementa.352, 2019.
 - Platt, U., and Stutz, J.: Differential Optical Absorption Spectroscopy: Principles and Applications, Springer-Verlag, Berlin Heidelberg, 2008.
- Pöhler, D., Vogel, L., Friess, U., and Platt, U.: Observation of halogen species in the Amundsen Gulf, Arctic, by active long-path differential optical absorption spectroscopy, Proceedings of the National Academy of Sciences of the United States of America, 107, 6582–6587, https://doi.org/10.1073/pnas.0912231107, 2010.
 - Pratt, K. A., Custard, K. D., Shepson, P. B., Douglas, T. A., Pöhler, D., General, S., Zielcke, J., Simpson, W. R., Platt, U., Tanner, D. J., Gregory Huey, L., Carlsen, M., and Stirm, B. H.: Photochemical production of molecular bromine in Arctic surface snowpacks, Nature Geoscience, 6, 351–356, https://doi.org/10.1038/ngeo1779, 2013.
- Ranjithkumar, A., Duncan, E., Yang, X., Partridge, D. G., Lachlan-Cope, T., Gong, X., Nishimura, K., and Frey, M. M.: Direct observation of Arctic Sea salt aerosol production from blowing snow and modeling over a changing sea ice environment, Elem Sci Anth, 13, https://doi.org/10.1525/elementa.2024.00006, 2025.
 - Rayner, N. A., Parker, D. E., Horton, E. B., Folland, C. K., Alexander, L. V., Rowell, D. P., Kent, E. C., and Kaplan, A.: Global analyses of sea surface temperature, sea ice, and night marine air temperature since the late nineteenth century, Journal of Geophysical Research: Atmospheres, 108, 4407, https://doi.org/10.1029/2002jd002670, 2003.
 - Richter, A., Wittrock, F., Eisinger, M., and Burrows, J. P.: GOME observations of tropospheric BrO in northern hemispheric spring and summer 1997, Geophysical Research Letters, 25, 2683–2686, https://doi.org/10.1029/98gl52016, 1998.
 - Rodgers, C. D.: Inverse methods for atmospheric sounding, theory and practice, Series on Atmospheric, Oceanic and Planetary Physics, edited by Taylor, F. W., World Scientific, https://doi.org/10.1142/3171, 2000.
- Rozanov, A., Bovensmann, H., Bracher, A., Hrechanyy, S., Rozanov, V., Sinnhuber, B.-M., Stroh, F., and Burrows, J. P.: NO₂ and BrO vertical profile retrieval from SCIAMACHY limb measurements: Sensitivity studies, Adv. Space Res., 36, 846–854, https://doi.org/10.1016/j.asr.2005.03.013, 2005.
 - Rößler, T., Stein, O., Heng, Y., Baumeister, P., and Hoffmann, L.: Trajectory errors of different numerical integration schemes diagnosed with the MPTRAC advection module driven by ECMWF operational analyses, Geosci. Model Dev., 11, 575–592, https://doi.org/10.5194/gmd-11-575-2018, 2018.



855

860

865



- Salawitch, R. J., Canty, T., Kurosu, T., Chance, K., Liang, Q., da Silva, A., Pawson, S., Nielsen, J. E., Rodriguez, J. M., Bhartia, P. K., Liu, X., Huey, L. G., Liao, J., Stickel, R. E., Tanner, D. J., Dibb, J. E., Simpson, W. R., Donohoue, D., Weinheimer, A., Flocke, F., Knapp, D., Montzka, D., Neuman, J. A., Nowak, J. B., Ryerson, T. B., Oltmans, S., Blake, D. R., Atlas, E. L., Kinnison, D. E., Tilmes, S., Pan, L. L., Hendrick, F., Van Roozendael, M., Kreher, K., Johnston, P. V., Gao, R. S., Johnson, B., Bui, T. P., Chen, G., Pierce, R. B., Crawford, J. H., and Jacob, D. J.: A new interpretation of total column BrO during Arctic spring, Geophysical Research Letters, 37, L21805, https://doi.org/10.1029/2010gl043798, 2010.
- Sander, R., Keene, W. C., Pszenny, A. A. P., Arimoto, R., Ayers, G. P., Baboukas, E., Cainey, J. M., Crutzen, P. J., Duce, R. A., Hönninger, G., Huebert, B. J., Maenhaut, W., Mihalopoulos, N., Turekian, V. C., and Van Dingenen, R.: Inorganic bromine in the marine boundary layer: a critical review, Atmos. Chem. Phys., 3, 1301–1336, https://doi.org/10.5194/acp-3-1301-2003, 2003.
- Schmale, J., Arnold, S. R., Law, K. S., Thorp, T., Anenberg, S., Simpson, W. R., Mao, J., and Pratt, K. A.: Local Arctic Air Pollution: A Neglected but Serious Problem, Earth's Future, 6, 1385–1412, https://doi.org/10.1029/2018ef000952, 2018.
- Schofield, R., Johnston, P. V., Thomas, A., Kreher, K., Connor, B. J., Wood, S., Shooter, D., Chipperfield, M. P., Richter, A., von Glasow, R., and Rodgers, C. D.: Tropospheric and stratospheric BrO columns over Arrival Heights, Antarctica, 2002, Journal of Geophysical Research: Atmospheres, 111, D22310, https://doi.org/10.1029/2005jd007022, 2006.
- Schroeder, W. H., Anlauf, K. G., Barrie, L. A., Lu, J. Y., Steffen, A., Schneeberger, D. R., and Berg, T.: Arctic springtime depletion of mercury, Nature, 394, 331–332, https://doi.org/10.1038/28530, 1998.
- Seo, S., Richter, A., Blechschmidt, A.-M., Bougoudis, I., and Burrows, J. P.: First high-resolution BrO column retrievals from TROPOMI, Atmospheric Measurement Techniques, 12, 2913–2932, https://doi.org/10.5194/amt-12-2913-2019, 2019.
- Sihler, H., Platt, U., Beirle, S., Marbach, T., Kühl, S., Dörner, S., Verschaeve, J., Frieß, U., Pöhler, D., Vogel, L., Sander, R., and Wagner, T.: Tropospheric BrO column densities in the Arctic derived from satellite: retrieval and comparison to ground-based measurements, Atmospheric Measurement Techniques, 5, 2779–2807, https://doi.org/10.5194/amt-5-2779-2012, 2012.
- Simpson, W. R., von Glasow, R., Riedel, K., Anderson, P., Ariya, P., Bottenheim, J., Burrows, J., Carpenter, L. J., Frieß, U.,
 Goodsite, M. E., Heard, D., Hutterli, M., Jacobi, H.-W., Kaleschke, L., Neff, B., Plane, J., Platt, U., Richter, A., Roscoe,
 H., Sander, R., Shepson, P., Sodeau, J., Steffen, A., Wagner, T., and Wolff, E.: Halogens and their role in polar boundarylayer ozone depletion, Atmos. Chem. Phys., 7, 4375–4418, https://doi.org/10.5194/acp-7-4375-2007, 2007a.
 - Simpson, W. R., Carlson, D., Hönninger, G., Douglas, T. A., Sturm, M., Perovich, D., and Platt, U.: First-year sea-ice contact predicts bromine monoxide (BrO) levels at Barrow, Alaska better than potential frost flower contact, Atmos. Chem. Phys., 7, 621–627, https://doi.org/10.5194/acp-7-621-2007, 2007b.
 - Simpson, W. R., Brown, S. S., Saiz-Lopez, A., Thornton, J. A., and Glasow, R.: Tropospheric halogen chemistry: sources, cycling, and impacts, Chem Rev, 115, 4035–4062, https://doi.org/10.1021/cr5006638, 2015.



885

895

905



- Simpson, W. R., Peterson, P. K., Frieß, U., Sihler, H., Lampel, J., Platt, U., Moore, C., Pratt, K., Shepson, P., Halfacre, J., and Nghiem, S. V.: Horizontal and vertical structure of reactive bromine events probed by bromine monoxide MAX-DOAS, Atmospheric Chemistry and Physics, 17, 9291–9309, https://doi.org/10.5194/acp-17-9291-2017, 2017.
- Steffen, A., Douglas, T., Amyot, M., Ariya, P., Aspmo, K., Berg, T., Bottenheim, J., Brooks, S., Cobbett, F., Dastoor, A., Dommergue, A., Ebinghaus, R., Ferrari, C., Gardfeldt, K., Goodsite, M. E., Lean, D., Poulain, A. J., Scherz, C., Skov, H., Sommar, J., and Temme, C.: A synthesis of atmospheric mercury depletion event chemistry in the atmosphere and snow, Atmos. Chem. Phys., 8, 1445–1482, https://doi.org/10.5194/acp-8-1445-2008, 2008.
- 890 Steffen, A., Bottenheim, J., Cole, A., Ebinghaus, R., Lawson, G., and Leaitch, W. R.: Atmospheric mercury speciation and mercury in snow over time at Alert, Canada, Atmospheric Chemistry and Physics, 14, 2219–2231, https://doi.org/10.5194/acp-14-2219-2014, 2014.
 - Stein, A. F., Draxler, R. R., Rolph, G. D., Stunder, B. J. B., Cohen, M. D., and Ngan, F.: NOAA's HYSPLIT atmospheric transport and dispersion modeling system, Bull. Amer. Meteor. Soc., 96, 2059–2077, https://doi.org/10.1175/BAMS-D-14-00110.1, 2015.
 - Stutz, J., Thomas, J. L., Hurlock, S. C., Schneider, M., von Glasow, R., Piot, M., Gorham, K., Burkhart, J. F., Ziemba, L., Dibb, J. E., and Lefer, B. L.: Longpath DOAS observations of surface BrO at Summit, Greenland, Atmospheric Chemistry and Physics, 11, 9899–9910, https://doi.org/10.5194/acp-11-9899-2011, 2011.
- Thalman, R. and Volkamer, R.: Temperature dependent absorption cross-sections of O₂-O₂ collision pairs between 340 and 900 630 nm and at atmospherically relevant pressure, Phys Chem Chem Phys, 15, 15371–15381, https://doi.org/10.1039/c3cp50968k, 2013.
 - Theys, N., Van Roozendael, M., Errera, Q., Hendrick, F., Daerden, F., Chabrillat, S., Dorf, M., Pfeilsticker, K., Rozanov, A., Lotz, W., Burrows, J. P., Lambert, J.-C., Goutail, F., Roscoe, H. K., and De Mazière, M.: A global stratospheric bromine monoxide climatology based on the BASCOE chemical transport model, Atmos. Chem. Phys., 9, 831–848, https://doi.org/10.5194/acp-9-831-2009, 2009.
 - Theys, N., Van Roozendael, M., Hendrick, F., Yang, X., De Smedt, I., Richter, A., Begoin, M., Errera, Q., Johnston, P. V., Kreher, K., and De Mazière, M.: Global observations of tropospheric BrO columns using GOME-2 satellite data, Atmos. Chem. Phys., 11, 1791–1811, https://doi.org/10.5194/acp-11-1791-2011, 2011.
- Toyota, K., McConnell, J. C., Lupu, A., Neary, L., McLinden, C. A., Richter, A., Kwok, R., Semeniuk, K., Kaminski, J. W.,
 Gong, S.-L., Jarosz, J., Chipperfield, M. P., and Sioris, C. E.: Analysis of reactive bromine production and ozone depletion in the Arctic boundary layer using 3-D simulations with GEM-AQ: inference from synoptic-scale patterns, Atmos. Chem. Phys., 11, 3949–3979, https://doi.org/10.5194/acp-11-3949-2011, 2011.
 - Toyota, K., McConnell, J. C., Staebler, R. M., and Dastoor, A. P.: Air–snowpack exchange of bromine, ozone and mercury in the springtime Arctic simulated by the 1-D model PHANTAS Part 1: In-snow bromine activation and its impact on ozone, Atmos. Chem. Phys., 14, 4101–4133, https://doi.org/10.5194/acp-14-4101-2014, 2014.





- Tschudi, M. A., Meier, W. N., and Stewart, J. S.: An enhancement to sea ice motion and age products at the National Snow and Ice Data Center (NSIDC), The Cryosphere, 14, 1519–1536, https://doi.org/10.5194/tc-14-1519-2020, 2020.
- Tuckermann, M., Ackermann, R., Gölz, C., Lorenzen-Schmidt, H., Senne, T., Stutz, J., Trost, B., Unold, W., and Platt, U.: DOAS-observation of halogen radical-catalysed arctic boundary layer ozone destruction during the ARCTOC-campaigns 1995 and 1996 in Ny-Ålesund, Spitsbergen, Tellus B, 49, 533–555, https://doi.org/10.3402/tellusb.v49i5.16005, 1997.
- Vandaele, A. C., Hermans, C., Simon, P. C., Carleer, M., Colin, R., Fally, S., Merienne, M.-F., Jenouvrier, A., and Coquart, B.: Measurements of the NO₂ absorption cross-section from 42 000cm⁻¹ to 10 000 cm⁻¹ (238–1000 nm) at 220K and 294 K, J. Quant. Spectrosc. Radiat. Transf., 59, 171–184, https://doi.org/10.1016/S0022-4073(97)00168-4, 1998.
- Vogt, R., P. J. Crutzen, and R. Sander.: A mechanism for halogen release from sea-salt aerosol in the remote marine boundary layer, Nature, 383, 327–330, https://doi.org/10.1038/383327a0, 1996.
 - von Glasow, R., von Kuhlmann, R., Lawrence, M. G., Platt, U., and Crutzen, P. J.: Impact of reactive bromine chemistry in the troposphere, Atmos. Chem. Phys., 4, 2481–2497, https://doi.org/10.5194/acp-4-2481-2004, 2004.
 - von Glasow, R. and Crutzen, P. J.: Tropospheric Halogen Chemistry, in: Treatise on Geochemistry, vol. 4.02, edited by: Holland, H. D. and Turekian, K. K., Pergamon, Oxford, 1–67, https://doi.org/10.1016/B0-08-043751-6/04141-4, 2007.
- 930 Wagner, T. and Platt, U.: Satellite mapping of enhanced BrO concentrations in the troposphere, Nature, 395, 486–490, https://doi.org/10.1038/26723, 1998.
 - Wennberg, P.: Bromine explosion, Nature, 397, 299-300, 1999.
 - Wren, S. N., Donaldson, D. J., and Abbatt, J. P. D.: Photochemical chlorine and bromine activation from artificial saline snow, Atmospheric Chemistry and Physics, 13, 9789–9800, https://doi.org/10.5194/acp-13-9789-2013, 2013.
- Yian, P., Zhang, J., O'Neill, N. T., Toth, T. D., Sorenson, B., Colarco, P. R., Kipling, Z., Hyer, E. J., Campbell, J. R., Reid, J. S., and Ranjbar, K.: Arctic spring and summertime aerosol optical depth baseline from long-term observations and model reanalyses Part 1: Climatology and trend, Atmos. Chem. Phys., 22, 9915–9947, https://doi.org/10.5194/acp-22-9915-2022, 2022.
- Yang, X., Cox, R. A., Warwick, N. J., Pyle, J. A., Carver, G. D., O'Connor, F. M., and Savage, N. H.: Tropospheric bromine chemistry and its impacts on ozone: A model study, J. Geophys. Res., 110, D23311, https://doi.org/10.1029/2005JD006244, 2005.
 - Yang, X., Pyle, J. A., and Cox, R. A.: Sea salt aerosol production and bromine release: Role of snow on sea ice, Geophys. Res. Lett., 35, L16815, https://doi.org/10.1029/2008gl034536, 2008.
- Yang, X., Pyle, J. A., Cox, R. A., Theys, N., and Van Roozendael, M.: Snow-sourced bromine and its implications for polar tropospheric ozone, Atmos. Chem. Phys., 10, 7763–7773, https://doi.org/10.5194/acp-10-7763-2010, 2010.
 - Yang, X., Frey, M. M., Rhodes, R. H., Norris, S. J., Brooks, I. M., Anderson, P. S., Nishimura, K., Jones, A. E., and Wolff, E. W.: Sea salt aerosol production via sublimating wind-blown saline snow particles over sea ice: parameterizations and relevant microphysical mechanisms, Atmos. Chem. Phys., 19, 8407–8424, https://doi.org/10.5194/acp-19-8407-2019, 2019.





- Yang, X., Blechschmidt, A.-M., Bognar, K., McClure-Begley, A., Morris, S., Petropavlovskikh, I., Richter, A., Skov, H., Strong, K., Tarasick, D. W., Uttal, T., Vestenius, M., and Zhao, X.: Pan-Arctic surface ozone: modelling vs. measurements, Atmos. Chem. Phys., 20, 15937–15967, https://doi.org/10.5194/acp-20-15937-2020, 2020.
 - Yang, X., Strong, K., Criscitiello, A. S., Santos-Garcia, M., Bognar, K., Zhao, X., Fogal, P., Walker, K. A., Morris, S. M., and Effertz, P.: Surface snow bromide and nitrate at Eureka, Canada, in early spring and implications for polar boundary layer chemistry, Atmos. Chem. Phys., 24, 5863–5886, https://doi.org/10.5194/acp-24-5863-2024, 2024.
 - Zhao, X., Strong, K., Adams, C., Schofield, R., Yang, X., Richter, A., Friess, U., Blechschmidt, A.-M., and Koo, J.-H.: A case study of a transported bromine explosion event in the Canadian high arctic, J. Geophys. Res.-Atmos., 121, 457–477, https://doi.org/10.1002/2015JD023711, 2016.
- Zilker, B., Richter, A., Blechschmidt, A.-M., von der Gathen, P., Bougoudis, I., Seo, S., Bösch, T., and Burrows, J. P.:

 Investigation of meteorological conditions and BrO during ozone depletion events in Ny-Ålesund between 2010 and 2021,

 Atmos. Chem. Phys., 23, 9787–9814, https://doi.org/10.5194/acp-23-9787-2023, 2023.